

Capacity Characterization of a MIMO-OFDM Wireless Channel with BLAST Implementation

by

Jaimal Soni

A thesis
presented to the University of Waterloo
in fulfillment of the
thesis requirement for the degree of
Master of Applied Science
in
Electrical and Computer Engineering

Waterloo, Ontario, Canada, 2010

©Jaimal Soni 2010

I hereby declare that I am the sole author of this thesis. This is a true copy of the thesis, including any required final revisions, as accepted by my examiners.

I understand that my thesis may be made electronically available to the public.

Abstract

As the data rates and performance of current telecommunications technologies reach their limits, MIMO offers promising results allowing for higher spectral efficiencies (or capacities) through the use of multiple element antennas (MEAs). Conventional testing methods, however, cannot be used for multi-antenna systems due to the co-dependence of antenna and RF effects, and baseband hardware and software design. This dissertation specifies a novel MIMO-OFDM, BLAST-based testing design using a hybrid FPGA/DSP development platform from Lyrtech. The design allows for rapid implementation and a consistent indication of the channel impulse response. In addition, a multipath environment is further created to mimic a realistic high scattering scenario. A study of MIMO system capacity is performed along with measurements of an actual over-the-air (OTA) channel. Observations about capacity and the effect of MEA antenna separations are then drawn and conclusions made as to the overall ability to effectively test MIMO systems. The platform used is the result of efforts from several individuals within UW's CST group. My contributions and research are documented in this dissertation.

Acknowledgements

I would like to extend my gratitude and thanks to Dr. Amir Khandani. His expertise in the field of information theory and telecommunications make his research group one of the best in Canada. I am humbled to be given the opportunity to develop my research interests under his supervision. His welcoming and approachable nature have also made my graduate studies an enjoyable experience.

I would like to acknowledge Raphael, Mohsen, Ethan, Hamed, Arash, Sandra and the rest of the CST group for their valuable assistance in my research and the writing of this thesis.

Thank you to my mum and dad, who have both sacrificed an immeasurable amount for their children. Their never-ending support and belief in me is the reason I am where I am today. I cannot thank my brother enough for always being there for me, and along with his wife Mona and son Thrishul, showing me that true wealth lies in family. Thank you to my grandfather, Bapu, who has served as a role model for me throughout my life. Both my grandfather and grandmother, Masi, have given me unconditional support and instilled in me dedication and discipline to do whatever I undertake well.

I am further indebted to Professor Bill Bishop and Professor Pin-Han Ho for reading my thesis on such short notice and for your valuable insights. Thank you for all the help.

Lastly I would like thank my friends for making it all worthwhile. Thank you to Tariq, James, Christie and Dan, to whom I owe a great deal; Fahreen, Jason, Alan and Rajiv for the many great stories and experiences; and lastly Cynthia and Aly for their cherished friendship and encouragement.

To the most loving Father and Mother who always believed in me.

Contents

List of Tables	ix
List of Figures	xii
1 Introduction	1
1.1 Addressing Current Wireless Demands	2
1.2 Thesis Contributions	3
2 Background	5
2.1 Diversity	5
2.2 802.11	6
2.2.1 Modulation and Coding Schemes	6
2.2.2 Delay Spread and OFDM	7
2.2.3 Preamble	8
2.3 MIMO Systems	8
2.3.1 BLAST	9
2.3.2 Space-Time Coding	9
2.4 Related Research	10
3 A Study of Capacity	11
3.1 MIMO Capacity Formulation	11
3.2 Eigenvalue Decomposition of the Channel	12
3.3 CSI Known to Transmitter	14
3.4 Ergodic and Outage Capacity	14
3.5 Coherent Distance	15
3.6 OFDM-based MIMO	16

4	Research Contributions	17
4.1	Introduction	17
4.1.1	The Role of Scattering	17
4.1.2	Research Objective	18
4.2	Overview of Architecture	19
4.2.1	Physical Configuration	19
4.2.2	DSP Design (Receiver Only)	29
4.2.3	Safety Considerations	29
4.3	Testing Procedures	30
4.3.1	Procedure Summary	30
4.4	Results	34
4.4.1	Channel Characterization	35
4.4.2	MIMO Capacity	37
4.4.3	The Effect of Metallic Reflectors	37
4.4.4	Varying MEA Element Spacing	39
4.4.5	A Comparison to Previous Work	41
4.4.6	Design Challenges and Difficulties	41
5	Conclusions and Future Work	43
	Bibliography	45
	Appendix A: System Architecture	47
	Appendix B: Testing Procedure	51
	Appendix C: Additional Test Results	55

List of Tables

4.1	A summary of the equipment used for testing.	20
4.2	A summary of the test cases used in the study.	31
4.3	A summary of control registers.	32

List of Figures

2.1	Gains achieved from MIMO systems.[15]	6
2.2	Constellation mappings for for M=1, 4 and 16.[7]	7
2.3	An illustration of OFDM.	8
3.1	Decomposition of the channel to n eigenmodes [15].	13
3.2	The waterfilling method when CSI is known to transmitter.	14
4.1	An illustration of the Ring of Scattering propagation model.[15]	18
4.2	The division of the receiver and transmitter designs on the Lyrtech platform.	21
4.3	A Lyrtech node (receiver/transmitter).	21
4.4	A metallic reflector.	21
4.5	A topographical view of test environment and node placement.	22
4.6	Transmitter signals for 1 frame, including STS/LTS.	23
4.7	The relationship between gain setting and output power gain of RFFE.	24
4.8	Directivity patterns of chosen antennas.[20]	25
4.9	Key functional components of TX design.	26
4.10	Key functional components of receiver design.	26
4.11	The AC for a window size of 80 cycles.	27
4.12	An illustration of distance variation at receiver and transmitter.	30
4.13	A summary of the testing procedure used in the study.	32
4.14	Signals of interest for system calibration.	33
4.15	An overview of the received frame.	34
4.16	A comparison of channel coefficient for 2 experiments and 3 OFDM tones.	36
4.17	A frequency response of h_{22} for 3 experiments.	37
4.18	Eigenmode gains for $n=4$, OFDM Tone 1.	38
4.19	Capacity for several multipath experiments, OFDM Tone 1.	38
4.20	A comparison of average capacity with and without reflectors.	39

4.21	A comparison of average capacity for $d=1$ in, 3 in, and 5 in., OFDM Tone 1.	40
4.22	A comparison of average eigenmode gains for $d=1$ in, 3 in, and 5 in., OFDM Tone 1.	40
4.23	A comparison of average capacity for $d=1$ in, 3 in, and 5 in., OFDM Tone 52.	41
5.1	A schematic of a node's internal components and buses.	47
5.2	The Xilinx block-based TX design.	48
5.3	The Xilinx block-based RX design.	49
5.4	The Simulink block-based DSP design at the RX.	50
5.5	VHS Control Utility screenshot, programming the FPGA.	51
5.6	VHS Control Utility screenshot, setting control registers.	52
5.7	RFFE Utility screenshot.	53
5.8	Typical off-air received signals.	54
5.9	Eigenmode gains for $n=4$, OFDM Tone 26.	55
5.10	Eigenmode gains for $n=4$, OFDM Tone 52.	56
5.11	Capacity for several multipath experiments, OFDM Tone 26.	56
5.12	Capacity for several multipath experiments, OFDM Tone 52.	57

Chapter 1

Introduction

“The wireless telegraph is not difficult to understand. The ordinary telegraph is like a very long cat. You pull the tail in New York, and it meows in Los Angeles. The wireless is the same, only without the cat.”

—*Albert Einstein*

The advancement of telecommunications technology that we have seen since Marconi’s first wireless telegraph across the Atlantic is phenomenal. In the last decade or so, there has been a paradigm shift in the factors governing this advancement; what started off driven by military has grown into one of the largest consumer and enterprise-driven markets of our time. To summarize where we stand today with a single word (albeit with some difficulty)—mobility. A study conducted by the International Telecommunications Union (ITU) places the number of mobile subscribers in 2009 around the globe at 4.7 billion, up from 1.3 billion in 2003.[1] The same ITU study listed the percentage of the world’s population covered by cellular signal to be around 90%. These are impressive numbers to say the least. Coupled with mobile subscribers are over 1.9 billion Internet users across the globe. The Internet now transcends demographic, industry and application serving as a medium of effortlessly connecting people at opposite ends of the Earth. In a world of Blackberries, metro-wide Wifi hotspots and even consumer Internet service on airplanes, telecom has succeeded in ‘making the world a smaller place’.

When Bill Gates wrote his book, *The Road Ahead*, more than a decade ago, he spoke of technology that was radical at the time, much of which has now been realized and in everyday use. To get an idea of where telecom is heading, rather than describe what is currently available, it makes sense to describe what consumers and enterprises currently

want. In [2], Webb provides an appropriate summary of these wants: video communications wherever possible, whenever possible; unification of all messaging whereby a single message spans across all communications media; freedom to communicate anywhere, with any person; and lastly, the ability to communicate with any machine built now or in the future. It goes without saying that these wants should also be met in a simple, user-friendly manner and at a lower price point.

1.1 Addressing Current Wireless Demands

From the early analog cellular networks (also referred to as first generation) to the current 3G networks, telecom service providers are faced with the challenge of limited frequency spectrum and unforgiving wireless channel conditions. In addition, the evolution of wireless technology must be done economically, (i.e.; building off of older infrastructure rather than discarding it.) The current leading 3G cellular technology is UMTS (also known as WCDMA) and uses HSPA to achieve data rates of up to 8Mbps to 10 Mbps. For wireless LAN (W-LAN), 802.11a and HiperLAN2 achieve rates of up to 54Mbps through the use of technologies such as OFDM and dynamic frequency selection. The demands from the consumer and enterprise mentioned above would require data rates of 100 Mbps and above, especially for high-definition video transmission.[15]

To meet these demands, the current infrastructure needs to support even higher data rates and even better spectral efficiencies, notwithstanding the fact that the Quality of Service (QoS) and overall reliability of communications should improve. Further, integration of the services provided should be seamless—for instance, handover between networks should be transparent. The coverage spanned by networks should also be increased while infrastructure and operation costs are driven down. The conventional approach of increasing bandwidth is becoming increasingly difficult due to spectrum costs and regulations. Multiple-Input Multiple-Output (MIMO) technologies have proven to be promising in that they provide a way of improving the efficiency and performance of existing wireless links.

Preliminary integrations of MIMO technologies using multiple element antennas (MEAs) with HSPA push data rates to 20 Mbps. With the current evolution toward 4G technologies, the key distinction is a complete IP-based infrastructure. It was shown by Foschini in [3] that capacities of up to 42 bps/Hz (20 times the current) can be achieved using

Bell Labs Layered Space-Time (BLAST) techniques along with spatial division multiplexing (SDM). These techniques exploit spatial diversity in a high scattering environment to achieve astounding results. BLAST techniques can be integrated into existing W-LAN and cellular systems to provide impressive performance gains.

4G technologies, including 802.11n, Mobile WiMAX and Long-Term Evolution (LTE), have adopted MIMO technologies to offer significant performance improvements without any increased bandwidth uses. As is often the case, a tradeoff exists between performance and cost. MIMO technologies require a higher level of implementation complexity, greater costs and a higher time-to-market for many providers. In addition, conventional testing methodologies that separate signal and antenna characteristics from baseband and software designs cannot be used. MIMO presents new design and testing challenges as engineers strive to optimize product performance, often becoming barriers of entry for many researchers. It necessitates the use of a cross-functional design, from the antennas down to the baseband software components along with complex channel modeling and decoding algorithms. Further, over-the-air (OTA) testing is often necessary to produce usable testing results.[4]

MIMO channel modeling is an emerging area of research in an effort to optimize next generation telecommunication devices. It was shown by Foschini in [3] that the channel impulse can be modeled as a linear matrix of independent Gaussian transfer coefficients. In addition, MIMO efficiency is highly dependent on the level of correlation between spatially separated antennas. Smart antenna design along with a channel model incorporating spatial dependence can help bridge the gap between wireless demands and currently available infrastructure.

1.2 Thesis Contributions

The above observations serve as motivation for my research. This dissertation presents two key aspects of the research. It first specifies a novel way of implementing a realistic MIMO transceiver rapidly using a hybrid FPGA-DSP platform from Lyrtech. Previous implementations use software approaches that are difficult to implement in a consumer product, or warrant the usage of proprietary chips (or even fabricated ASICs). In addition, the system allows for OTA testing of a multipath environment, necessary for accurately studying a

MIMO wireless link. If needed, the design can utilize channel emulators, such as those from Azimuth, to test a variety of channel models and scenarios.

The second aspect of our research is a way of creating and studying a multipath channel with high scattering. Using two nodes placed 45' apart along with reflective metallic sheeting, a realistic multipath environment can be created. Channel impulse responses are measured and analyzed across frequency and spatial paths. Additionally, antenna element separations are a key factor in achieving spatial diversity. The capacity of this channel is analyzed for varying distances between antenna elements. This allows for a study of coherent distance in a device to minimize correlation between antennas and optimize performance. The impact of the presented research is thus the ability to test MIMO devices efficiently and effectively.

This thesis is organized as follows. Chapter 2 provides the necessary background information related to diversity and MIMO systems, fundamental concepts leading to major design decisions in our transceiver implementation, and related research. In Chapter 3, a study of system capacity for a MIMO channel is presented including its decomposition into parallel sub-channels. Chapter 4 details the implemented design and the multipath environment constructed, testing procedures for observing channel impulse response and capacity, and the results from this study. Finally, Chapter 6 provides conclusive remarks which summarize the contributions of this research topic and describe possible future work.

Chapter 2

Background

This chapter begins by outlining the fundamental concept behind modern wireless systems, namely diversity. Further, other concepts are described in a general sense so as to apply to all wireless systems. The most common standard for W-LAN communications at present is 802.11, starting with 802.11b, then revised as ‘a’, ‘g’ and most recently, ‘n’. Thus, through this standard the notion of modulation and coding schemes, delay spread due to multipath, OFDM, and preamble are summarized. Finally, advancements toward MIMO systems through BLAST implementations and space-time coding are discussed.

2.1 Diversity

Today’s telecommunications systems leverage diversity in an effort to maximize performance and QoS. Different channels are known to fade and be susceptible to interference independently. Thus, multiple versions of a message can be transmitted and/or received at the destination. This can be used in addition to forward error correction (FEC) codes to increase redundancy and guarantee a certain level of reliability. Alternatively, a message can be split and multiplexed across different channels to increase data rates.

The three best known diversity schemes are as follows. Frequency diversity is implemented by using channels at several orthogonal frequency bands simultaneously, such as in OFDM. Time diversity splits a desired message into different time slots. Space diversity sends a message over spatially different propagation paths. Our MIMO-OFDM implementation utilizes all three diversity schemes to maximize performance gain. This gain can be classified into two categories: antenna gains, or increases in average output SNR, and

diversity gains, or the decreases in SNR required to achieve a desired data rate. Spatial multiplexing further provides throughput gains. A generalized summary of MIMO gains is provided in Fig. 2.1.[5]

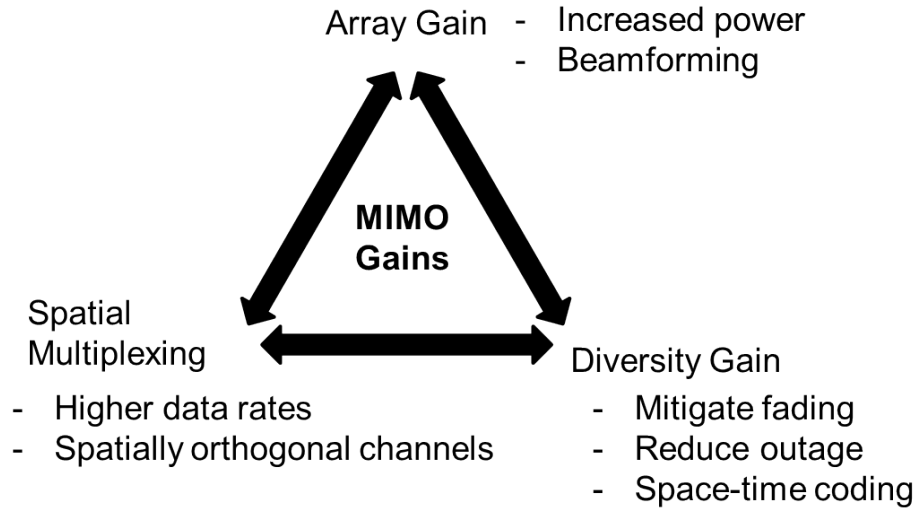


Figure 2.1: Gains achieved from MIMO systems.[15]

2.2 802.11

IEEE 802.11, or simply 802.11, is a widely accepted W-LAN standard for communications today. The initial specification utilized the 2.4 GHz ISM band (802.11b) and a 20 MHz bandwidth, with data rates up to 11Mbps. With the introduction of 802.11a, data rates of 54Mbps could be achieved. 802.11a uses OFDM and optionally the unlicensed 5 GHz spectrum. The specification defines several PHY-layer characteristics, a few of which are summarized in the subsequent sections. [6]

2.2.1 Modulation and Coding Schemes

As specified in the 802.11 specification, [7], OFDM subcarriers are modulated using rectangular quadrature amplitude modulation (QAM) schemes. A message is divided into groups of M bits, corresponding to the QAM mapping chosen where $M=1,2,4$ or 6 . A transmitted signal for a given mapping is referred to as a symbol. In addition grey-coding is used to maximize the Hamming distance between adjacent constellation points. Fig. 2.2

illustrates QAM mapping for $M=1$ (BPSK), 4 (4-QAM or QPSK), and 16-QAM.

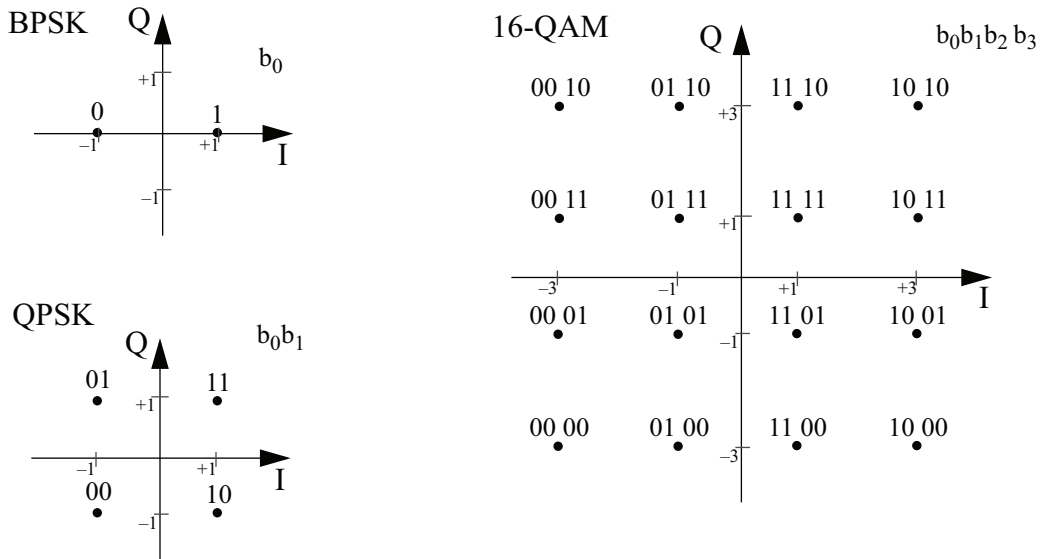


Figure 2.2: Constellation mappings for for $M=1$, 4 and 16.[7]

In addition to modulation, 802.11 specified methods for mitigating errors in transmission. Two of those methods are data interleaving and FEC coding. Data interleaving involves dispersing a message in time to combat burst errors. FEC coding involves the use of convolutional coding to add memory and redundancy to a message. Consequently, data can be decoded using Viterbi trellis coding even if a receiver has only part of the transmitted message. FEC brings with it the cost of lower data rates with the benefit of higher link reliability.

2.2.2 Delay Spread and OFDM

In realistic wireless propagation environments, a received signal at the destination is comprised of the original transmitted signal and several instances of signals reflected off the receiver's surroundings. This creates a multipath spread, or delay spread with a given power delay profile. If the delay spread is comparable to the symbol duration, in time, overlapping of symbols will occur causing inter-symbol interference (ISI). To combat ISI, a guard interval is introduced known as a cyclic prefix.

In the frequency domain, ISI corresponds to frequency-dependent fading. The absence

of ISI produces flat fading. For wideband signals, OFDM can be used to divide up the allotted spectrum into several parallel sub-channels. The result is a ‘flatter’ fading environment across each narrowband sub-channel. OFDM warrants the use of an IFFT functional block that spreads N_{fft} data symbols into a combined time-domain OFDM symbol of period N_{fft} . This time-domain is comprised of N_{fft} frequency subcarriers, each carrying a data symbol. The process in the frequency-domain is illustrated in Fig. 2.3.

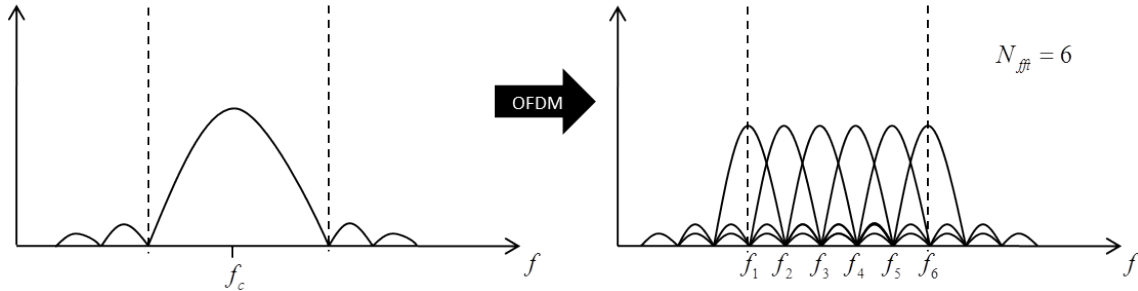


Figure 2.3: An illustration of OFDM.

It is important to note that a message is broken up into frames comprised of a fixed number of OFDM symbols in length. The symbol period is calculated as 50 ns for a bandwidth of 20 MHz. The length of an OFDM symbol is 4 μ s, 3.2 μ s for data ($N_{fft}=64$) and 0.8 μ s for a guard interval.

2.2.3 Preamble

The 802.11 preamble consists of several components facilitating the transmission and decoding of a frame. The short training sequence (STS) allows for signal detection, AGC calibration and coarse frequency offset estimation, while the long training sequence (LTS) allows for channel estimation and fine frequency estimation. In addition, a signal field provides details on the coding and modulation schemes used for the frame to the receiver. A detailed description on the 802.11 preamble can be found in [7].

2.3 MIMO Systems

As mentioned above, MIMO systems leverage space diversity to achieve higher QoS for the end user. N_R antennas at the transmitter send a frame that is received by M_T receiver

antennas. In [3], Foschini describes an early adoption of MIMO into a wireless link, namely Bell Labs Layered Space-Time (BLAST). The implementation in the subsequent chapters of this dissertation adapt these techniques.

2.3.1 BLAST

A technique for implementing a high spectral efficiency system using MEAs was first proposed in [3], referred to as BLAST. The technique exploits multipath environment and de-correlation of propagation paths in a fading channel, contrary to conventional SISO systems where multipath was considered detrimental to signal recovery. It is important to note that the bandwidth and total power used are the same as a 1x1 (SISO) implementation. At the receiver, advanced signal processing and decoding methods are used to estimate the transmitted signal. The implementation proposed in this research employs zero-forcing with successive interference cancellation (ZF-SIC). Further details on ZF-SIC can be found in [9].

BLAST simplifies the transmitter and receiver architecture by eliminating FEC and advanced modulation schemes. The implementation combines techniques specified in 802.11, such as OFDM and training sequences, to produce a real-time OTA platform. BPSK was used throughout all testing.

2.3.2 Space-Time Coding

Capacities proposed in [10] and [11] are theoretical in nature—practically unattainable without the use of an adequate coding scheme. It is shown in [12], that capacities close to the theoretical capacity limit can be achieved through methods involving sending multiple redundant copies of a message across spatially orthogonal paths. The resulting scheme is referred to as either space-time trellis coding (STTC) or space-time block coding (STBC). Our implementation of a MIMO-OFDM platform includes support for STBC and the use of a combiner at the receiver. All testing, however, was done with this disabled as it is beyond the scope of this study.

2.4 Related Research

In [13], high scattering environments are modelled for a BLAST system and a study of antenna separation on capacity is presented. It presents early results as to the effect of antenna correlation on system performance. MIMO systems promise to provide high spectral efficiencies leading to significant improvements in data rates. This claim, however, exists with one caveat: the spectral efficiency is severely reduced if the arriving signals at the receiving antennas are correlated. It was shown that the antenna separation of $\lambda/2$ can theoretically achieve near complete de-correlation. This paper also integrates correlation of receive and transmit antennas into a capacity formulation. A 16x16 MIMO, BLAST-based system was shown to achieve a capacity of 42 bps/Hz at 10 dB SNR.

A 3x3 MIMO-BLAST implementation is presented [14], including necessary changes to a conventional SISO baseband design. This includes modifications to time synchronization, channel estimation and frame detection and decoding. The system was implemented using FPGAs to store pre-encoded data at the transmitter for transmission and then at the receiver to store off-air signals for post-processing. Performance of the system was benchmarked against a 1x1 counterpart, demonstrating a doubling of throughput for the 3x3 system. It was also shown that the maximum gain factor of 3 was only achievable in favourable MIMO channels where correlation was minimized.

In any practical test environment, a real-time OTA study is crucial in optimizing device performance. The related studies present simulation results for capacity and its dependence on antenna spacing. They further specify a design allowing for OTA studies, but not real-time indications of channel performance; all frame generation and data analysis is done off-air. Our research builds on both studies, first by designing a real-time 4x4 MIMO transceiver using a rapid development platform, and then by studying the channel response and capacity of the link for different antenna spacings.

Chapter 3

A Study of Capacity

The starting point for this research finds itself at the theoretical upper bound on the transmission rate for a SISO system, referred to as Shannon capacity. Transmitting higher than this rate, regardless of channel and source coding chosen, and regardless of modulation scheme introduces errors into the transmission. This capacity is given in Eq. (3.1) for a channel bandwidth B , signal power P and noise power N_0 . For completeness, Eq. (3.2) shows that the capacity is also equal to the mutual information between input X and output Y to a channel.

$$C = B \log_2 \left(1 + \frac{P}{N_0 B} \right) \quad (3.1)$$

$$C = \sup_{p(x)} I(X; Y) \quad (3.2)$$

3.1 MIMO Capacity Formulation

In a MIMO system, the transmitted signal is a $M_T \times 1$ column vector, \mathbf{s} , with each element, s_i , an i.i.d. Gaussian variable. Assuming equal power distribution between s_i 's gives rise to the following correlation matrix:

$$\mathbf{R}_{ss} = \frac{E_s}{M_T} I_{M_T} \quad (3.3)$$

Assume a narrowband channel, providing a flat frequency response. In the case of a wideband signal, OFDM can be used to divide the channel into several sub-channels to achieve this goal, as shown in Section 2.2.2. The channel response is modeled with a $N_R \times M_T$ matrix of complex fading coefficients; $h_{i,j}$ is the coefficient from the j th transmitter antenna to the i th receiver antenna. Signal noise is modelled as a $N_R \times 1$ vector of zero mean

circularly symmetrical complex Gaussian variables (ZMCSCG) with variance N_0 . Finally, we express the correlation matrix of the $N_R \times 1$ noise vector as the following:

$$\begin{aligned}\mathbf{R}_{nn} &= E[\mathbf{nn}^H] \\ &= N_0 \mathbf{I}_{N_R}\end{aligned}\tag{3.4}$$

Assume that the received power is the same as the transmitted power, E_s , as gains and power levels can be adjusted in a real-world application to meet this criteria. Thus the SNR is simply E_s/N_0 .

As shown in [15], the system can be modelled as the following:

$$\mathbf{y} = \mathbf{H}\mathbf{s} + \mathbf{n}\tag{3.5}$$

Where, \mathbf{y} is the received signal, \mathbf{H} is the channel impulse response and \mathbf{n} is the additive noise. The capacity of the system, or the upper bound on the virtually error-free transmission rate, is then defined as:

$$C = \max_{f(\mathbf{s})} I(\mathbf{s}; \mathbf{y})\tag{3.6}$$

As proven in [10,11], this is approximated by:

$$C = \max_{tr(\mathbf{R}_{ss}) \leq P} \log_2 \left[\det \left(\mathbf{I}_{N_R} + \mathbf{H}\mathbf{R}_{ss}\mathbf{H}^H \right) \right] \text{ bps/Hz}\tag{3.7}$$

In the case where knowledge of the channel is known only at the receiver, \mathbf{s} is chosen to maximize Eq. (3.6) making $\mathbf{R}_{ss} = (E_s/M_T)\mathbf{I}_{M_T}$, justifying the earlier assumption of equal power distribution between transmitters. This capacity simplifies to:

$$C = \log_2 \left[\det \left(\mathbf{I}_{N_R} + \frac{E_s}{M_T N_0} \mathbf{H}\mathbf{H}^H \right) \right] \text{ bps/Hz}\tag{3.8}$$

3.2 Eigenvalue Decomposition of the Channel

The practical significance of a MIMO system lies in the ability to conceptually separate the MIMO channel into SISO sub-channels. The number of sub-channels n is equal to $\min(N_R, M_T)$ as shown in Fig. 3.1.

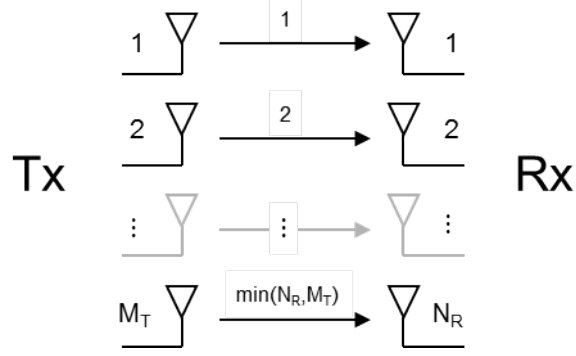


Figure 3.1: Decomposition of the channel to n eigenmodes [15].

It follows that the system capacity can be expressed as the sum of the individual capacities. Using singular value decomposition, express the channel matrix as:

$$\mathbf{H} = \mathbf{U}\mathbf{D}\mathbf{V}^H \quad (3.9)$$

\mathbf{D} is a diagonal matrix with the singular values of \mathbf{H} being the diagonal elements. These singular values are also equivalent to the square roots of the eigenvalues. It can further be shown that decomposition of $\mathbf{H}\mathbf{H}^H$ leads to the following capacity equation:

$$C = \log_2 \left[\det \left(I_{N_R} + \frac{p_i}{N_0} \mathbf{U}\mathbf{\Lambda}\mathbf{U}^H \right) \right] \text{ bps/Hz} \quad (3.10)$$

Where \mathbf{U} is a positive semi-hermitian matrix having $\mathbf{U}^H\mathbf{U} = \mathbf{U}\mathbf{U}^H = I_{N_R}$ and $\mathbf{\Lambda} = \text{diag}\{ \lambda_1 \ \lambda_2 \ \dots \ \lambda_{N_R} \}$. It follows that:

$$\begin{aligned} C &= \log_2 \left[\det \left(I_{N_R} + \frac{p_i}{N_0} \mathbf{\Lambda} \right) \right] \text{ bps/Hz} \\ &= \sum_{i=1}^n \log_2 \left[I_{N_R} + \frac{p_i}{N_0} \lambda_i \right] \text{ bps/Hz} \end{aligned} \quad (3.11)$$

subject to,

$$\begin{aligned} \lambda_i &= \begin{cases} \sigma_i^2, & i = 1, 2, \dots, n \\ 0, & i = n + 1, \dots, N_R \end{cases} \\ \sum_{i=1}^n p_i &= P \end{aligned} \quad (3.12)$$

The above formulation assumes no channel state information (CSI) at the transmitter. In addition, the eigenvalues can be interpreted as the relative gains on each parallel sub-

channel. Eqs. (3.11) & (3.12) imply that the power on ‘mode’ i is represented by the weighting p_i and bounded by the total power constraint P . With no CSI, $p_i = P/n$. Capacities higher than that shown in 3.11 can be achieved if knowledge of the eigenmode gains—CSI—can be fed back to the transmitter as shown in the next section.

3.3 CSI Known to Transmitter

CSI can be attained at the transmitter primarily by two methods: feedback from the receiver or assuming a reciprocal channel in a bi-directional wireless link. Once CSI is available to the MIMO transmitter, capacities above Eq. (3.11) can be attained using the ‘Water-filling’ algorithm.

Water-filling as shown in [16] and [9] involves deriving an optimization problem and then using Lagrangian methods to find optimum power-levels for each channel mode such that system capacity is maximized. Fig. 3.2 illustrates the concept of waterfilling, where μ is the waterlevel and the p_i^{opt} 's are the optimal power weightings for each mode. The capacity is again given by Eq. 3.11, but in this case equal power distribution is not necessarily the case.

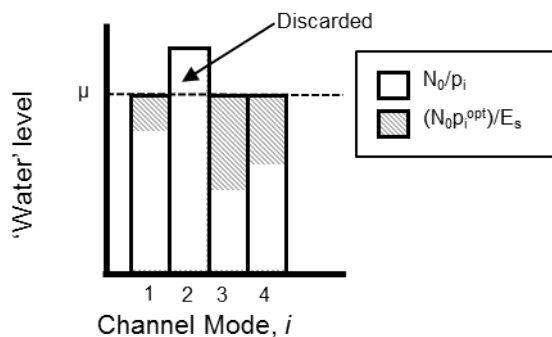


Figure 3.2: The waterfilling method when CSI is known to transmitter.

3.4 Ergodic and Outage Capacity

The capacity formulation above is for a given realization of a MIMO channel and its coefficients. This capacity is loosely called the ‘instantaneous’ capacity of the system and represents the maximum rate or spectral efficiency one can attain to have the BER and

FER arbitrarily small [17]. In some environments, it is possible to make the assumption that the channel changes slow enough so as to deem the channel matrix constant for one or more frames. In this case, the instantaneous capacity becomes the capacity for a single realization of the channel, valid for the entire frame duration[15]. For this study, assume that the channel is slow fading. It is shown in [15] that this is a reasonable assumption for most 802.X-based applications. Ergodic capacity is a more general case where every realization of the channel response is independent, with no correlation to any previous realization. The capacity is taken as the ensemble average, assuming the process is ergodic—the result of an infinite number of measurements—and is expressed as:

$$C = E \left\{ \sum_{i=1}^n \log_2 \left[I_{N_R} + \frac{p_i}{N_0} \lambda_i \right] \right\} \text{ bps/Hz} \quad (3.13)$$

In simulations, the MIMO channel is modelled as Rayleigh with the channel matrix elements being ZMCSCG i.i.d. random variables. As previously defined, capacity is the maximum rate at which information can be transmitted virtually error-free. In practical applications, outage capacity is defined as the capacity guaranteeing a certain level of reliability, r_0 , or $\Pr(C < C_0) = r_0$. Thus, for no errors, $r_0 \rightarrow 0$.

The outage capacity is often expressed as a commulative distribution function (CDF) to illustrate capacities for different reliabilities at a fixed SNR. As shown in [18], the formulation for the CDF of capacity for a Rayleigh MIMO channel takes the form of a complex phi function as shown in Eqn. 3.14. Often, however, Monte Carlo methods are used to plot the outage capacity of a system.

$$F_C(x) = \int_{-\infty}^{\infty} \phi_C(z) \left[\frac{1 - e^{-j2\pi zx}}{j2\pi z} \right] dz \quad (3.14)$$

3.5 Coherent Distance

As mentioned above, the MIMO channel matrix is mathematically modelled as Rayleigh with iid components. It was shown in [10] that to get independent fading in each of the antennas in a multiple element antenna (MEA), at least a half wavelength separation is required. The coherent distance is then, $d = \lambda/2$. Often due to a poor scattering environments and shadowing, larger separations are required. As shown in [9], the capacity

of the MIMO system taking into account correlation between MEA elements is:

$$C \approx \log_2 \left[\det \left(\frac{E_s}{M_T N_0} \mathbf{H}_\omega \mathbf{H}_\omega^H \right) \right] + \log_2 [\det(\mathbf{R}_r)] + \log_2 [\det(\mathbf{R}_t)] \text{ bps/Hz} \quad (3.15)$$

For cellular implementations, base stations' incoming signals might be highly correlated due to a narrow angular spread. It is usually, however, feasible to attain separations of 10 to 16 wavelengths as is often the case. The mobile handset has a better scattering environment, but separation is often limited to the coherent distance or only slightly larger. Thus we can assume correlation only at the receiver; the correlation matrix is shown in Eq. (3.16). Note that $\log_2 [\det(\mathbf{R}_r)] \leq 0$, making it a reduction in Eq. (3.15) as expected.[9]

$$\mathbf{R}_r = \begin{bmatrix} 1 & \sigma \\ \sigma & 1 \end{bmatrix}; \quad \sigma \leq 1 \quad (3.16)$$

3.6 OFDM-based MIMO

OFDM ensures a narrowband channel by splitting the wideband channel into N parallel sub-channels. Each subchannel is orthogonal to the others and lies on a different subcarrier. It was shown in [17], that the capacity of an OFDM-based MIMO system is simply the mean of the capacities on each subcarrier as seen in:

$$C = \frac{1}{N} \sum_{k=1}^N \log_2 \left[\det \left(I_{N_R} + \frac{E_s}{M_T N_0} \mathbf{H}_k \mathbf{H}_k^H \right) \right] \text{ bps/Hz} \quad (3.17)$$

Chapter 4

Research Contributions

4.1 Introduction

This chapter begins with a discussion on the role of scattering. It subsequently provides details on the research motivation and objective. The architecture of the implemented platform is then described along with the testing procedures used. Finally, the results from the conducted tests are shown.

4.1.1 The Role of Scattering

There are a number of propagation models used to characterize a MIMO Wireless Channel. Exploiting these models to achieve higher diversity gains is a large area of research in telecommunications. The key concept in each is that in addition to the line-of-sight (LOS) signal sent by a transmitter, several other signals may arrive at the receiver at different times and at different angles. These ‘scatterers’ mostly occur at the mobile station (MS) or at the base station (BS) from objects at similar heights surrounding each. Consequently, the multipath effect is modeled by a time and frequency dependent channel impulse response, $h_\omega(t, \tau)$. In a MIMO system, the channel impulse becomes an $N_R \times M_T$ transfer matrix \mathbf{H} .

A simple method for modeling scatterers at the MS is known as the ‘Ring of Scatterers’. It is shown in [15] that scattering at the MS can be decomposed into discrete clusters of effective scatterers uniformly spaced around the circumference of a circle as shown in Fig. 4.1.

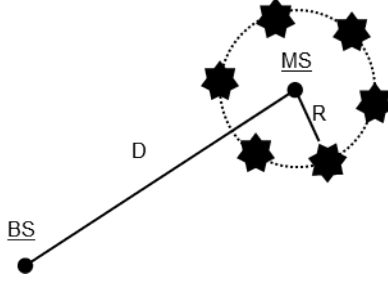


Figure 4.1: An illustration of the Ring of Scatterers propagation model.[15]

The Ring of Scatterers assumes a narrow angular spread at the BS and high scattering leading to a wide angular spread at the MS. The angles of arrivals at the MS are given by Eq. (4.1), where N is the number of scatterers, R is the distance of each cluster from the MS and D is the distance between the MS and BS.

$$\theta_i = \frac{R}{D} \sin\left(\frac{2\pi}{N}i\right), i = 1, \dots, N \quad (4.1)$$

MIMO systems leverage highly scattering environments to achieve high spectral efficiencies. This is due to the uncorrelated nature of the signal observations at each receiver antenna in an ideal case, improving diversity gain. In any practical cellular implementation, the base station is typically placed above most of the local infrastructure that scatter the incoming signal. As a result the incident angular spread is relatively narrow. This implies that received signals are not completely uncorrelated. Alternatively, the angular spread at the mobile station is significantly wider. Geographical conditions, man-made structures, cars and people all contribute to a high level of scattering around the mobile handset. Thus, our research approximates the propagation model to the ‘Ring of Scatters’.[15,13]

4.1.2 Research Objective

In studying the theoretical capacity of a MIMO system, it is necessary to mimic a realistic scattering environment to produce fruitful results. Thus, the first objective would be to design a layout that positions a transmitter far enough away from a receiver node to attain a similar multipath result. In addition to this, a MIMO wireless receiver and transmitter need to be constructed that are able to transmit a predetermined signal from one point to another. Lastly, a method of measurement needs to be designed along with appropriate metrics chosen to allow for a coherent study of the wireless link and its channel character-

istics.

The ultimate research objective is to study the capacity of a 4×4 MIMO link. With the above mentioned system implemented, the first goal is to find a consistent way of attaining the channel capacity, one that conforms to previous literature studies. The second goal is to study one of the key factors affecting this channel capacity—the spacing between antenna elements at (either the receiver or transmitter nodes). The following sections outline the test platform implementation and the testing environment along with the results from the research study.

4.2 Overview of Architecture

4.2.1 Physical Configuration

This section outlines the implemented MIMO platform. It begins with the major design decisions and subsequently provides further details where needed.

4.2.1.1 Major Design Decisions

In designing and implementing a 4×4 MIMO-OFDM transceiver, several design decisions were made. This included hardware and antenna selection, along with the separation of the design into DSP and FPGA components.

4.2.1.1.1 Hardware Selection

The equipment to construct each node is listed in Table 4.1. These choices were made prior to the start of our research; all but the antenna selection and metal sheeting were already purchased and available for use.

4.2.1.1.2 Separation of design into FPGA and DSP

The major functional requirements of the transmitter were as follows: generation of data, conversion to OFDM, adding training sequences and outputting a signal to the RFFE. The major functional requirements of the receiver design were as follows: time synchronization, frequency/phase offset compensation, conversion from OFDM, channel estimation and MIMO decoding.

Table 4.1: A summary of the equipment used for testing.

Equipment	Qty.	Description/Role
FPGA/DSP-based Development Platform	2	A platform developed by Lyrtech containing a fully-functional PC with a FPGA board and a hybrid FPGA/DSP board each connected via the cPCI bus. Appropriate software was loaded onto the PC to run the node along with LAN connectivity.
RFFE	2	RF front-end units developed by ComLab serving as the complete baseband to carrier solution. This included upconversion and gain control.
Signal Generator	2	Used to create an 80 MHz master clock to drive the FPGA designs; the DSPs ran on an internal 1 GHz clock.
Mobile	4	Mobile stands used to maneuver around the metallic reflectors.
Antenna	8	Omnidirectional antennas specified for use in 2.4 GHz and 5 GHz bands produced by L-com.
Metal Sheeting & stand	6	Used as reflectors to improve scattering at the receiver.
Oscilloscope & stand	1	Used to monitor signals of interest for calibration at the receiver.
WLAN Spectrum Monitor	6	A software-based tool to aid in channel selection to minimize unwanted interference from other band users.
ESD Mat	2	Mats produced by 3M to prevent electrostatic discharge.

FPGA design offers the advantage of strict timing calibration and analysis capabilities, and better performance, while DSP offers the advantage of quicker and less complex development. The ZF-SIC algorithm used for MIMO decoding is an iterative process involving complex math—difficult to build on an FPGA. Thus, ZF-SIC decoding was implemented on a DSP while the remainder of the design was implemented in a FPGA. Fig. 4.2 summarizes the division of the design.

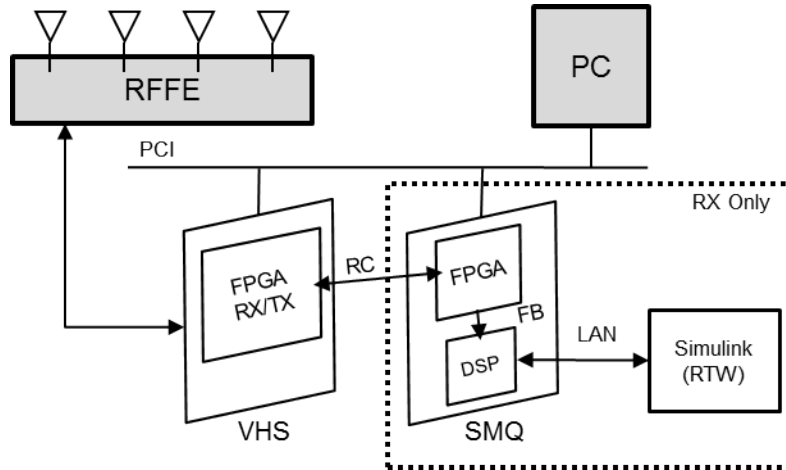


Figure 4.2: The division of the receiver and transmitter designs on the Lyrtech platform.

4.2.1.1.3 Node Placement and Environment

As described in Section 4.1.1, the environment in which the tests were conducted aimed at mimicking a realistic scattering scenario. Testing was conducted in the CST Lab, comprised of two adjacent rooms, at the University of Waterloo; nodes were placed on either end, spaced 45' apart. Metallic reflectors were used around the receiver to improve scattering. A topographical view of the test environment is shown in Fig 4.5.

The reflectors (shown as dotted lines in Fig. 4.5) were made of sheet metal and placed on mobiles, while the nodes were placed on stationary tables atop ESD mats. Figs. 4.3 and 4.4 depict a transmitter/receiver node and a reflector respectively.

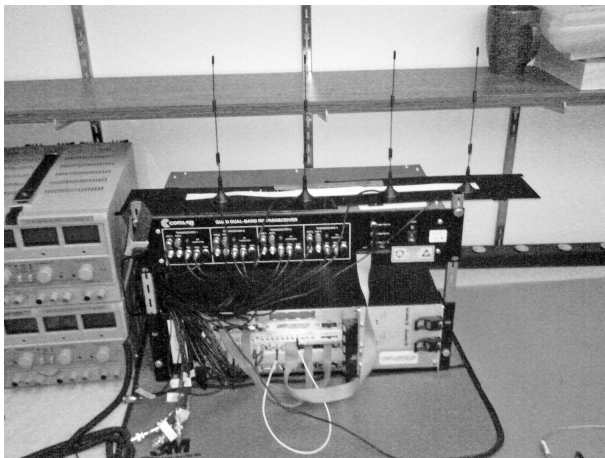


Figure 4.3: A Lyrtech node (receiver/transmitter).

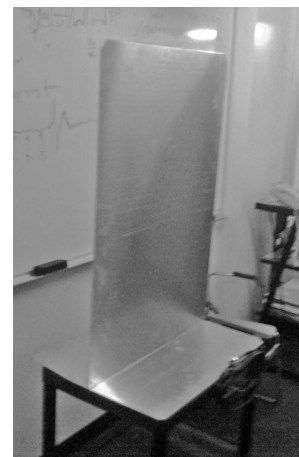


Figure 4.4: A metallic reflector.

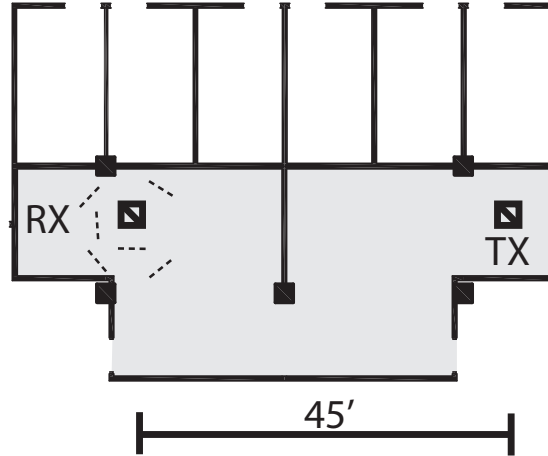


Figure 4.5: A topographical view of test environment and node placement.

4.2.1.1.4 Time Synchronization and Channel Estimation

The receiver design loosely follows the 802.11X specification for time synchronization as shown in [7]. Both a short and long training sequence (STS and LTS) are prepended to the payload data prior to transmission of each frame as shown in Fig. 4.6. The STS is used to generate a ‘Start of Frame’ (SOF) that enables succeeding processing blocks. The LTS is used to estimate the channel coefficients to characterize the channel impulse response. To attain all 16 paths in the 4×4 MIMO system, the LTS is sent 4 times, each orthogonal in time and space to one another. Further details on receiver design are provided in Section 4.2.1.2.2.

4.2.1.1.5 Signal Bandwidth

The bandwidth of the channel follows the 802.11a specification of 20 MHz listed in [7]. The FPGA design at the transmitter can generate data at 80 MHz, which is then demultiplexed into 4 streams at 20 MHz and sent to each of the transmitting antennas. The RFFE provides appropriate filtering for noise and interference suppression. At the receiver, 4 streams of data are then multiplexed and upsampled once again to 80 MHz.

4.2.1.1.6 Hardware Characterization

The Lyrtech nodes provide a robust development environment for a number of applications. Each node contains a main Xilinx Virtex4 FPGA board called the VHS, programmable via a utility on the attached PC. The boards include 8 A/D, D/A converters and 128 MB of onboard SDRAM. An additional 8 A/D, D/A converters can be added through the use of a

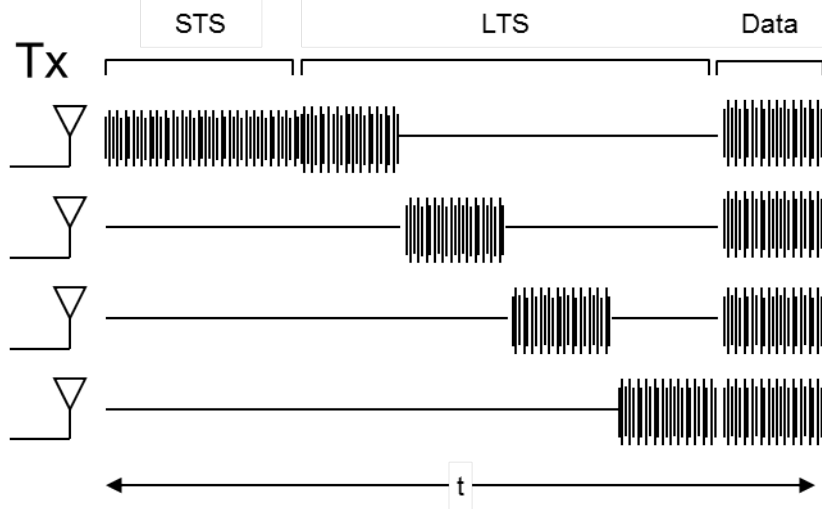


Figure 4.6: Transmitter signals for 1 frame, including STS/LTS.

daughterboard. Each node also contains a hybrid FPGA/DSP board containing two clusters called the Signal Master Quad (SMQ). Both clusters provide a Xilinx Virtex4 FPGA, 2 DSPs and 128 MB SDRAMs. The SMQ and VHS boards each contain PCI controllers for communication with the attached control PC; the SMQ additionally has an Ethernet LAN controller.

All FPGA cores are driven by an external 80 MHz clock, downsampled within the FPGA design as needed, while the DSP contains an internal 1 GHz processor. Further details about the internal architecture and bus speeds are illustrated in Fig. 5.1. Section 4.2.1.1.7 provides further details about communication between components and interfaces.

The ComLab RF front-end (RFFE) units provide a complete solution including base-band (IF) to carrier upconversion, and programmable gain control. Each unit contains 4 ports that can each be configured as transmitter or receiver and as one of 2 polarities. Gains can be applied to each of the ports independently. Each unit increase in gain setting corresponds to approximately 2 dBm in power gain [19]. Fig. 4.7 illustrates the relationship between gain setting and output power gain.

4.2.1.1.7 Hardware Interfacing

There are 4 main communication buses used: Rapid Channel (RC) between the VHS and SMQ's FPGA cores, Fast Bus (FB) between a SMQ cluster's FPGA core and a DSP, cPCI

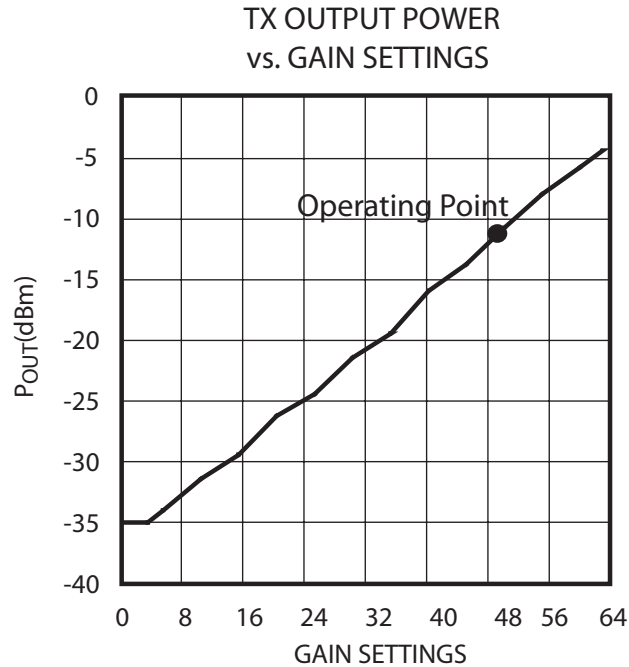


Figure 4.7: The relationship between gain setting and output power gain of RFFE.

between the boards and the control PC, and Ethernet for communication over LAN. The RC bus is 64 bits in width and runs at 500 MHz. This allows for the entire FPGA design (SMQ and VHS) to run at 80 MHz. The SMQ’s FB is 32 bits in width and runs at 100 MHz. Although the DSP runs at 1 GHz, the transmission overhead and processing time necessitate the use of data buffering in the SMQ FPGA design. The PCI bus is 64 bits in width and runs at 66 MHz—adequate as this bus is solely used to initially program the FPGA cores and set control registers. Finally, the SMQ uses an Ethernet controller to enable real-time communication over LAN with each DSP. Lyrtech’s Real-Time Workshop platform allows for remote programming of a DSP along with feedback, much like a simulation would run.

4.2.1.1.8 Antenna characterization

It was specified that each of the 8 antennas should produce a high level of scattering at the height of each node. In addition, the antennas should be matched in impedance for maximum transmission power. Thus, a $50\ \Omega$ monopole, omni-directional antenna was chosen. Fig. 4.8 illustrates the directivity pattern of the antenna.

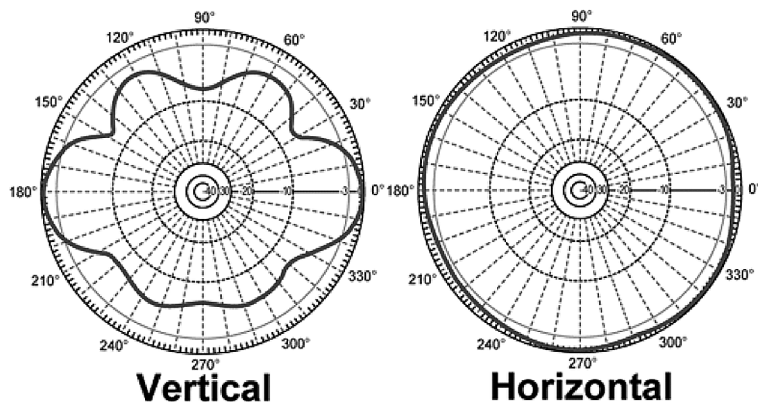


Figure 4.8: Directivity patterns of chosen antennas.[20]

4.2.1.2 FPGA Design

Most of the baseband design was implemented on FPGA due to performance requirements. The following sections outline the Transmitter and Receiver parts. DSP was used only for the receiver’s MIMO decoding and is outlined in the subsequent section.

4.2.1.2.1 Transmitter

The key functional components of transmitter are summarized in Fig. 4.9. Additionally Fig. 5.2 provides a screenshot of the actual block-based FPGA design. In Fig. 4.9, the data is generated at random (or alternatively fixed for BER calculation) at the receiver. Each frame carries 4 OFDM symbols of data, along with the added STS and LTS signals. There were $N_{fft} = 64$ OFDM carrier tones used, 4 of which carried pilot symbols for tracking at the receiver and 12 of which carried zero and DC components. Thus, there were 48 data symbols per OFDM symbol $N_{NDSC} = 48$. Lastly, the length of an OFDM symbol in time was 64 cycles. A cyclic prefix of 16 cycles was added to form a guard interval to combat ISI.

4.2.1.2.2 Receiver

The key functional components of the receiver are summarized in Fig. 4.10. Additionally Fig. 5.3 provides a screenshot of the actual block-based FPGA design. The design is divided into VHS and SMQ components below.

VHS

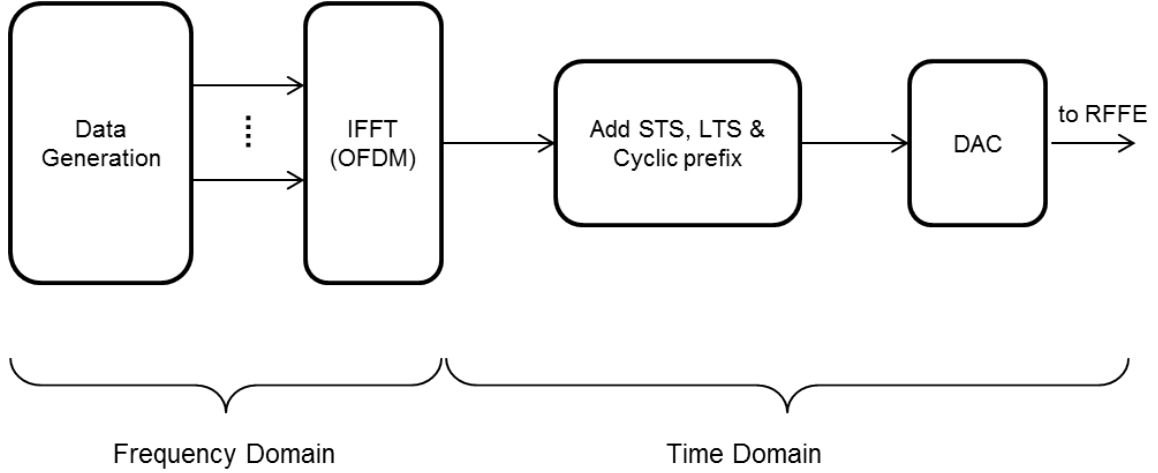


Figure 4.9: Key functional components of TX design.

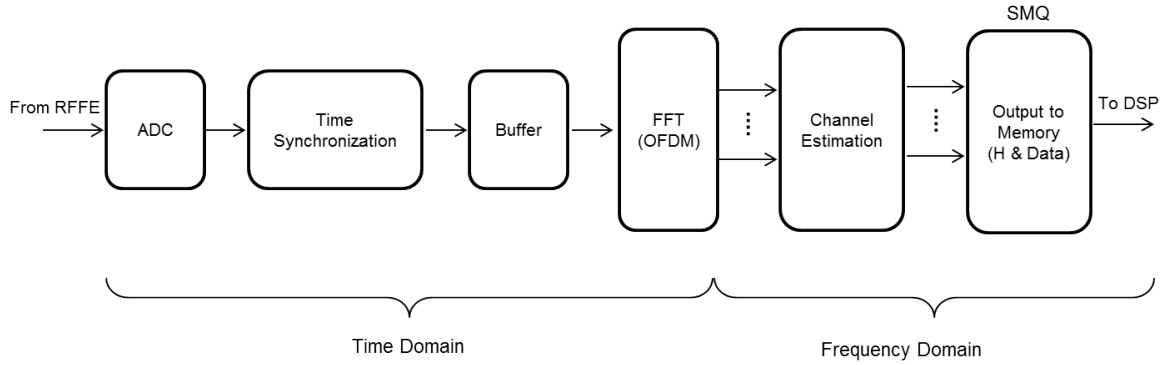


Figure 4.10: Key functional components of receiver design.

Time synchronization is performed at the receiver through the use of the STS as specified in [21]. A SOF signal is generated through the use of a normalized (auto)correlation (AC) between the received signal and a delayed version of itself. Defining the complex correlation between two observations of the received signal of length of N_c as

$$\begin{aligned}
 \Lambda(\tau) &= \sum_{n=\tau-(N_c-1)}^{\tau} \mathbf{r}^H(n - N_c)\mathbf{r}(n) \\
 &= \sum_{n=\tau-(N_c-1)}^{\tau} \sum_{i=1}^{N_R} r_i^*(n - N_c)r_i(n)
 \end{aligned} \tag{4.2}$$

The received power is then

$$\begin{aligned}
 P(\tau) &= \sum_{n=\tau-(N_c-1)}^{\tau} \mathbf{r}^H(n)\mathbf{r}(n) \\
 &= \sum_{n=\tau-(N_c-1)}^{\tau} \sum_{i=1}^{N_R} r_i^*(n)r_i(n)
 \end{aligned} \tag{4.3}$$

Using the maximum-normalized-correlation (MNC) criterion demonstrated in [14], the SOF is given by

$$SOF = \arg \max_{\tau} \left[\frac{\sum_{j=1}^{M_T} 4|\Lambda(\tau_j)|^2}{\sum_{j=1}^{M_T} P(\tau_j - N_c)^2 + P(\tau_j)^2} \right]; SOF \geq r_{AC} \tag{4.4}$$

Where $\tau_j = \tau - (N_T - j)N_{STS}$, $N_{STS}=64$ cycles and $N_c=80$ cycles. Thus, using an AC window size of 80 cycles, the SOF is triggered after its value is held above a certain threshold, r_{AC} , for 64 cycles as illustrated in Section 4.11. r_{AC} is adjusted based on the signal power using control registers during system calibration.

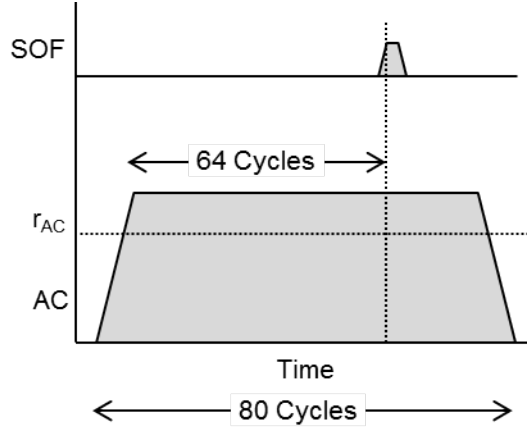


Figure 4.11: The AC for a window size of 80 cycles.

Following time synchronization, data is buffered then passed through an FFT to produce the received frequency-domain (FD) signal. The received LTS can be used to estimate the channel impulse response in the following way. Using the system model shown in Eq. (3.5), it is shown in [14] that after FFT the FD received signal can be represented by the

following:

$$\hat{\mathbf{x}}_{i,j} = \begin{pmatrix} x_{i,j}(0) \\ \vdots \\ x_{i,j}(N_{fft} - 1) \end{pmatrix} \quad (4.5)$$

The number of OFDM tones is $N_{fft} = 64$. In addition, it is possible to identify the signal in Eq. (4.5) as being received on receiver antenna i from transmitter antenna j due to the orthogonality in time and space of the LTS. It is further shown that using an LTS as defined in [7]

$$\hat{\mathbf{x}}_{i,j} = \mathbf{D} \begin{pmatrix} h_{i,j}(0) \\ \vdots \\ h_{i,j}(N_{fft} - 1) \end{pmatrix} + \mathbf{n}_{i,j} \quad (4.6)$$

where $\mathbf{n}_{i,j}$ is the FD noise term. Estimating the channel coefficients is simply

$$\mathbf{h}_{i,j}^{est} = \begin{pmatrix} h_{i,j}^{est}(0) \\ \vdots \\ h_{i,j}^{est}(N_{fft} - 1) \end{pmatrix} = \mathbf{D}^H \hat{\mathbf{x}}_{i,j} \quad (4.7)$$

Note that the pseudo-inverse of \mathbf{D} simplifies to its Hermitian transpose for a diagonal matrix. The above leads the following channel matrix for a 4x4 MIMO implementation

$$\mathbf{H} = \begin{bmatrix} h_{1,1}^{est} & h_{2,1}^{est} & h_{3,1}^{est} & h_{4,1}^{est} \\ h_{1,2}^{est} & h_{2,2}^{est} & h_{3,2}^{est} & h_{4,2}^{est} \\ h_{1,3}^{est} & h_{2,3}^{est} & h_{3,3}^{est} & h_{4,3}^{est} \\ h_{1,4}^{est} & h_{2,4}^{est} & h_{3,4}^{est} & h_{4,4}^{est} \end{bmatrix} \quad (4.8)$$

After time synchronization, FFT and channel estimation, the above channel coefficients are sent to the SMQ along with the payload over FB.

SMQ

Data is sent to the SMQ via the RC bus, and then channeled to one of the SMQ DSPs via the FB interface. The off-air data is also recorded into the on-board SDRAM; this data is saved to the attached PCs harddisk for further processing off-line.

4.2.2 DSP Design (Receiver Only)

For testing and MIMO link verification, a full baseband decoder was implemented. ZF-SIC decodes the layered space-time signal by exploiting the channel response to select the strongest path and decoding this first. The decoded signal is then removed from the received signal and the process is repeated [10]. To gauge performance, the received symbols were compared with known transmitted symbols to get an indication of bit-error-rate (BER). A screenshot of the DSP block-based design is depicted in Fig. 5.4.

To perform further analysis, such as channel response characterization and capacity measurement, a secondary DSP design was created. This design solely contained the control blocks to capture off-air data from the on-board SDRAM. This off-air data consisted of the raw channel coefficients for 16 paths and 48 OFDM data tones in addition to the payload data for a predetermined number of frames.

4.2.3 Safety Considerations

Throughout the implementation and testing conducted in this research, a significant amount of care was put into the safety of the individuals involved and that of the equipment used. Two main considerations were electrostatic discharge and maximum transmit power.

4.2.3.0.3 Electrostatic Discharge

Both the FPGA/DSP development platform and the RFFE units were extremely sensitive to electrostatic discharge (ESD). As a result appropriate precautions were made when handling equipment. Each node was placed on a static dissipative mat and a wrist band worn to ground any stray static electricity the body might carry.

4.2.3.0.4 Maximum Transmit Power

Government regulatory bodies such as the FCC and CRTC specify maximum transmit power levels for 802.X-based systems. The typical range for 802.X is between -60 and -80 dBm. With maximum gain settings on the RFFE, the average transmit power observed

for our transmitted signal was between -80 and -100dBm —thus ensuring our design was within the regulation guidelines.

4.3 Testing Procedures

As previously described, the goal of this research is to get a consistent indication of the non-ergodic capacity of a 4×4 MIMO Channel. A preliminary study was conducted to characterize the channel for several multipath environments and measure the associated capacities. The study was then extended to study the effect of receiver Multiple Element Antenna (MEA) spacings—namely, 1 in., 3 in. and 5 in. The spacing was adjusted at both receiver and transmitter nodes as shown in Fig. 4.12

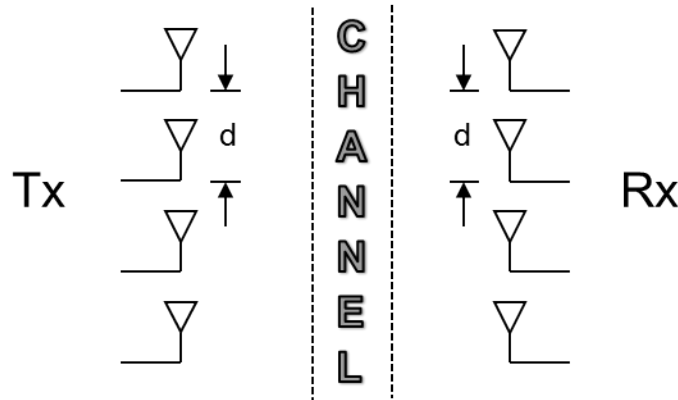


Figure 4.12: An illustration of distance variation at receiver and transmitter.

The system is comprised of two nodes (transmitter and receiver) with identical FPGA designs loaded onto each. The appropriate A/D and D/A configurations, front-end gains and design register values are set accordingly for each test. In addition, the receiver is also comprised of a DSP design. The subsequent sections summarize the testing procedure.

4.3.1 Procedure Summary

The environment used for all of the testing was the CST HCL Lab at the University of Waterloo. The physical placement of the receiver and transmitter nodes was fixed throughout and illustrated in Fig. 4.5. In addition, the 6 metallic reflectors were placed around the

receiver node to increase scattering at the mobile station.

In an effort to attain confident and repeatable results, 8 measurements were taken for each test case. For comparison, a set of test results were also recorded without any reflectors in place. Lastly, the antennas were kept in the same broadside arrangement and at the same height at both transmitter and receiver nodes. Table 4.3 summarizes the test cases used in the study.

Table 4.2: A summary of the test cases used in the study.

Test Case	Element Spacing	# of Experiments	Metallic Reflectors?
A	5 inches	8	Yes
B	5 inches	8	No
C	3 inches	8	Yes
D	1 inch	8	Yes

Fig. 4.13 summarizes the test procedure. The subsequent sections provide additional details as needed.

4.3.1.0.5 Preliminary Configuration

Prior to powering up the devices, an external signal generator was used to create a base clock of 80 MHz. The reflectors were placed around the receiver node at random to create a multipath environment, and the MEA element spacings set accordingly.

4.3.1.0.6 Loading FPGA and Registers for SISO

A Lyrtech utility was used to load the FPGA bitstream to each node and set the appropriate control register values. Figs. 5.5 and 5.6 contain screenshots of the utility.

4.3.1.0.7 Adjusting the RFFE

The FPGA design has a gain setting that can be used to boost the transmitted signal power. The RF front-end unit also provides a second stage of amplification. Fig. 4.7 illustrates the relationship between the gain setting and the signal amplification. In addition, the utility allows the baseband signal to be upconverted to the appropriate carrier for a specified 802.11 channel. It was found that Channel 9 contained the least amount of interference from other users; thus this channel was used for all measurements taken. The gain settings

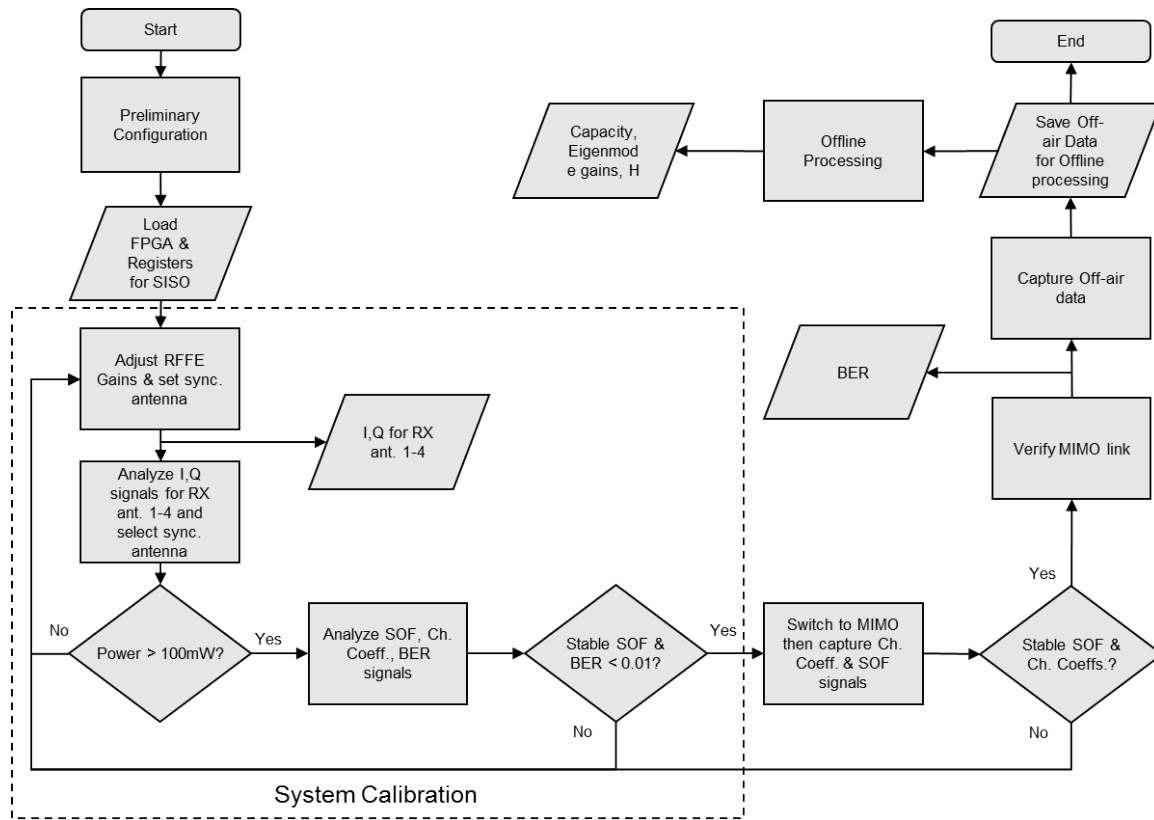


Figure 4.13: A summary of the testing procedure used in the study.

Table 4.3: A summary of control registers.

	Description
Register 1	Mode (SISO/MIMO); Synchronization antenna for STS; TX gain (Stage 1); FFT start delay
Register 2	Number of data symbols transmitted
Register 3	Output selection (I,Q or SOF, Channel Coefficients, Data and Errors); RX/TX selection
Register 4	AC (SOF) threshold

were manipulated to attain a stable SOF and channel coefficients; the measured SNR at the receiver front-end was approximately 20 dB. Fig. 5.7 provides a screenshot of the RFFE control utility.

4.3.1.0.8 Analyzing I,Q Signals

It was found that a stable Start of Frame (SOF) with minimal errors was only possible for signals having a power greater than 100mW. Thus, ensuring this is the case is a good starting point for calibration. A depiction of the typical received signals can be found in Fig 5.8. Additionally, the Short Training Sequence (STS) is sent off of one of the transmitter antennas and the synchronization done at the receiver of one—synchronization is essentially completed in a SISO fashion. Accordingly, the antennas used for each can be adjusted to aid calibration using control registers.

4.3.1.0.9 Analyzing SOF, Channel Coefficients and BER Signals

The goal of system calibration is to attain a stable SOF and channel coefficients, indicating that transmitted frames are being detected and decoded correctly. Fig. 4.14 illustrates the 4 main signals of interest when calibrating the system. Adjustments are made accordingly to gain and receiver/transmitter settings to attain stable signals as illustrated.

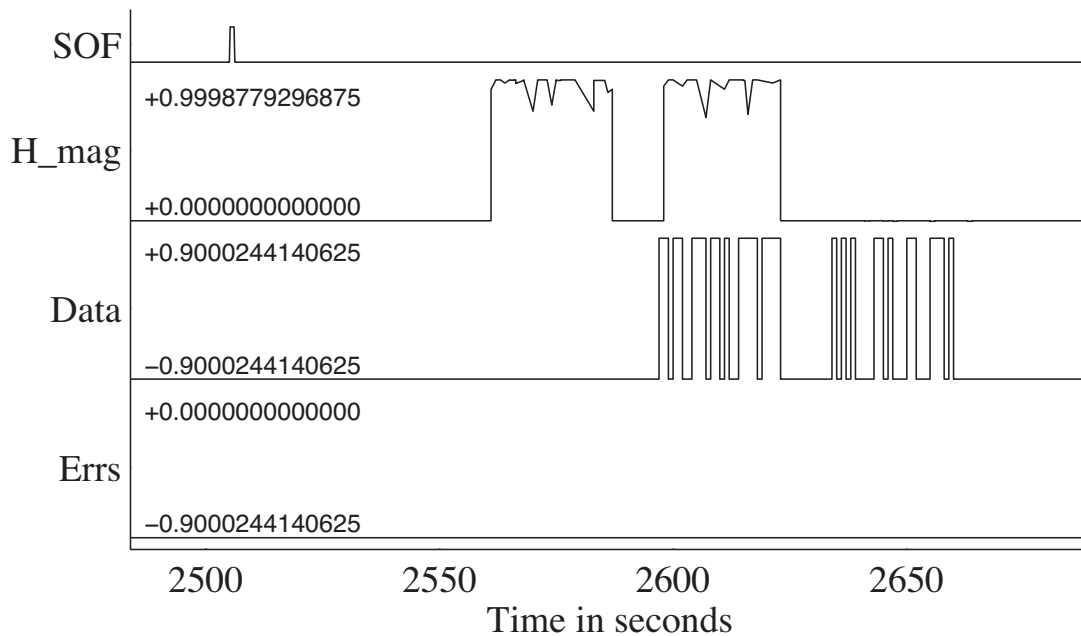


Figure 4.14: Signals of interest for system calibration.

4.3.1.0.10 Verifying MIMO link

Once calibrated, the system is set to MIMO mode, whereby data is sent on all four antennas simultaneously following a V-BLAST architecture. As described in Section 4.2.1.1.4, the LTS is sent orthogonally in time and space to attain the channel coefficients. To verify the MIMO link the Baseband Decoder DSP design is run in MATLAB Simulink, and connect to the running RX node. Fig. 5.4 provides a screenshot of the DSP design.

4.3.1.0.11 Off-air processing

After calibrating the system and verifying the MIMO link, the off-air data is stored for off-line processing. This allows for adequate analysis of the channel coefficients, MIMO channel eigenmode gains, and capacity measurements.

4.4 Results

The basis for our 4×4 MIMO system is a high scattering environment. Depending on the environment and its associated multipath effect, coefficients should vary significantly between experiments and between each other. As mentioned above, the baseband receiver design takes in a composite signal from the receiver frontend, comprised of in-phase and quadrature components. The signals at each receiving antenna represent the aggregate sum of each transmitted signal, and the effect of the channel and additive noise for each path. The baseband design then estimates the related channel coefficients for each OFDM tone and for every frame sent using training sequences. Each frame carries 4x4x52 coefficients in addition to the payload as illustrated in Fig. 4.15.

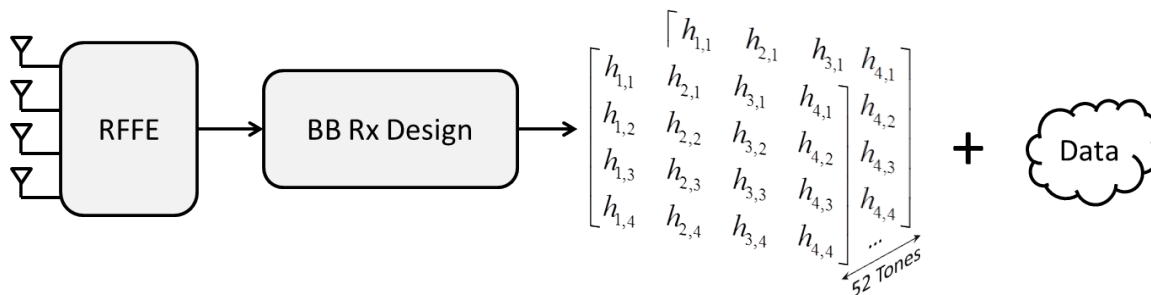


Figure 4.15: An overview of the received frame.

The results are organized as follows: The channel is first characterized in terms of channel coefficients and eigenmode gains. The measured capacity is then presented. Sub-

sequently, a study of the effect of MEA element spacing is provided. It is important to note that metallic reflectors were used in every experiment except where noted otherwise.

4.4.1 Channel Characterization

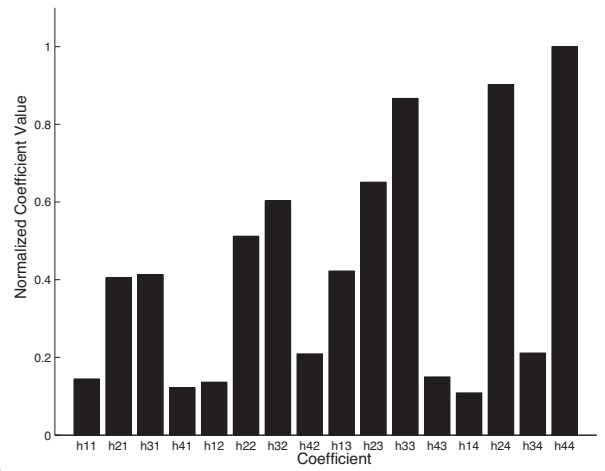
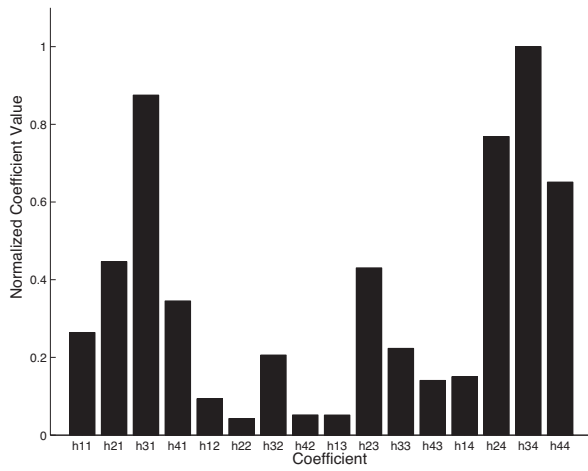
It was observed that the channel coefficients are in fact highly dependent on the multipath environment in which the tests are conducted. Fig. 4.16a displays these 16 coefficients for two experiments of test case A (OFDM Tone 1). The figure clearly illustrates that the channel coefficients vary significantly between the two displayed experiments. Figs. 4.16b and 4.16c illustrate this result for OFDM tones 26 and 52.

A frequency response is also of interest in characterizing the channel in an OFDM-based MIMO implementation. Fig. 4.17 illustrates the variation in channel coefficients of an given path, h_{22} , across 52 OFDM subcarriers for 3 different experiments.

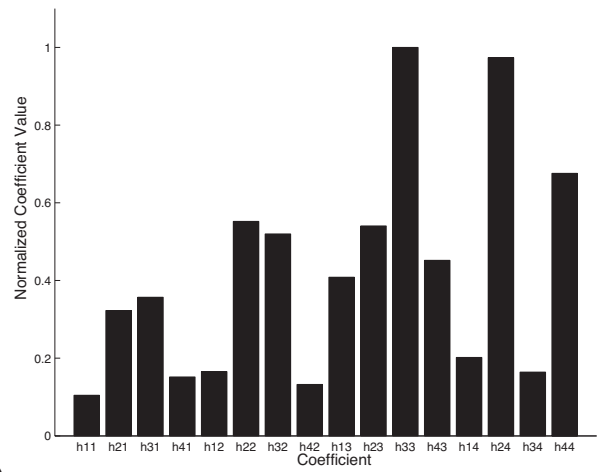
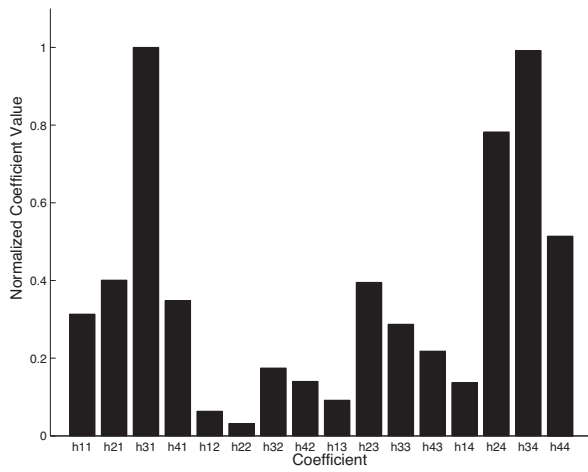
As described in Section 3.2, a channel realization can also be decomposed in terms of n eigenmodes with associated gains. Fig. 4.18 illustrates the eigenmode gains for several experiments on OFDM Tone 1, where in our case $n = \min(N_R, M_T) = 4$. Figs. 5.9 and 5.10 illustrate the results on Tones 26 and 52 for comparison.

Fig. 4.18 illustrates slight variations in eigenmode gains between experiments. Some consistency is observed throughout. Modes 1 and 2 appear to be significantly degraded by the channel, with mode 1 being completely eradicated. Modes 3 and 4 appear to be significantly higher in gain leading to a better sub-channel. This information can be exploited to achieve higher capacities with CSI at the transmitter and Waterfilling as shown in Section 3.3.

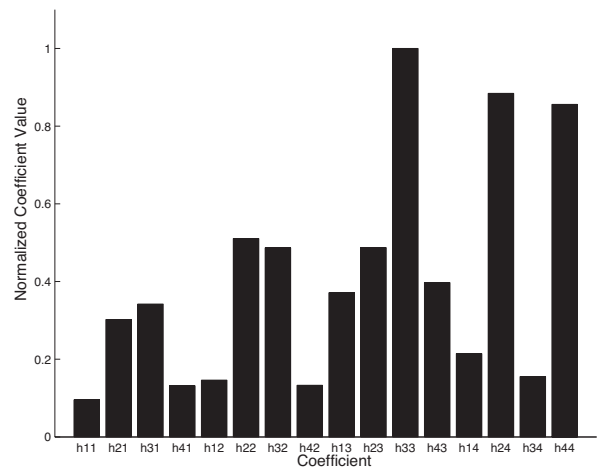
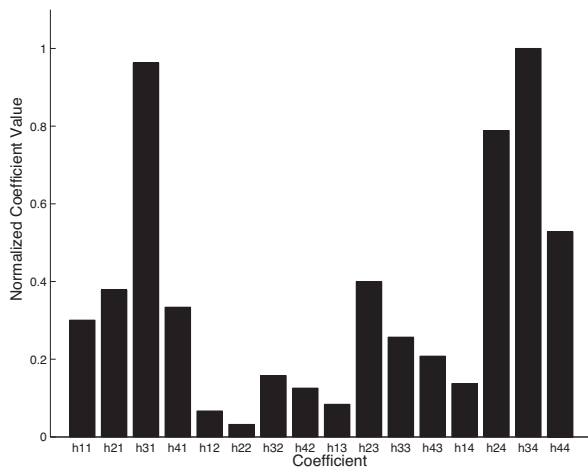
The above analysis provides evidence that varied multipath effects exist for each experiment due to the varied channel responses above. It is also shown through eigendecomposition, that some sub-channels are consistently weaker than others. This is true for cases where there exists some correlation between received signals due to a worse than ideal scattering environment. In the next section, it is illustrated that even though the channel responses vary, the capacity is nevertheless consistent between experiments.



a)



b)



c)

Figure 4.16: A comparison of channel coefficient for 2 experiments and 3 OFDM tones.

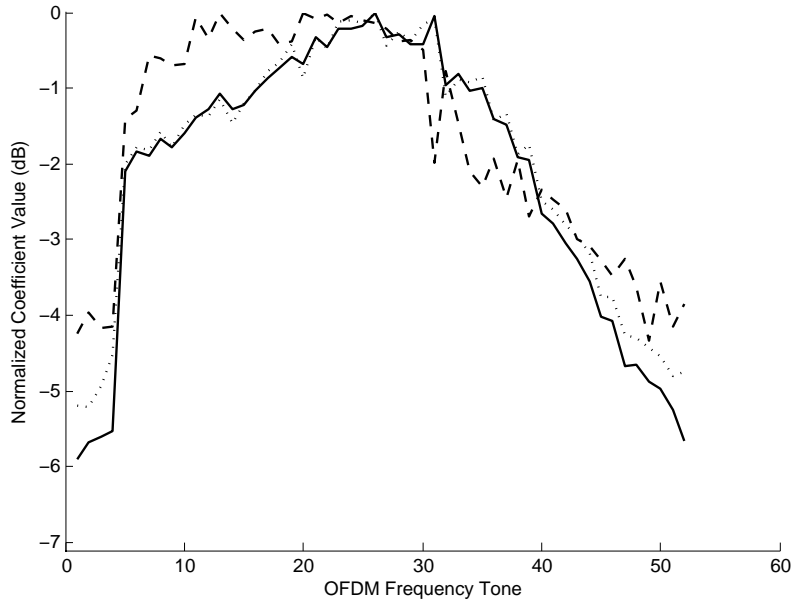


Figure 4.17: A frequency response of h_{22} for 3 experiments.

4.4.2 MIMO Capacity

As described in Section 4.3, several multipath environments were arranged and the channel response captured. After normalizing the channel coefficients as shown above, it is possible to get a channel matrix that characterizes the channel independent of the SNR. Thus, using Eqn. 3.11, the capacity for each measured channel realization can be plotted. As mentioned in Section 3.4, the channel is assumed to be fixed for the duration of a frame and non-ergodic capacity is plotted. Fig. 4.19 illustrates the capacity for Tone 1 for test case A (Tones 26 and 52 are shown in Fig. 5.11 and Fig. 5.12). It is observed that the capacity does in fact remain consistent between experiments. Note that as described in Eqn. 3.17, the total system capacity is in fact the mean of the capacities across all OFDM tones used.

4.4.3 The Effect of Metallic Reflectors

As mentioned above in Section 4.2.1.1.3, the receiver and transmitter were spatially placed such that there was no LOS signal path between them. The walls of the lab and other common building materials, however, are not perfect reflectors as shown in [22]. Consequently, metallic sheets were used to improve scattering at the receiver. Fig. 4.20 compares the average capacity for all experiments with reflectors to the average for all experiments

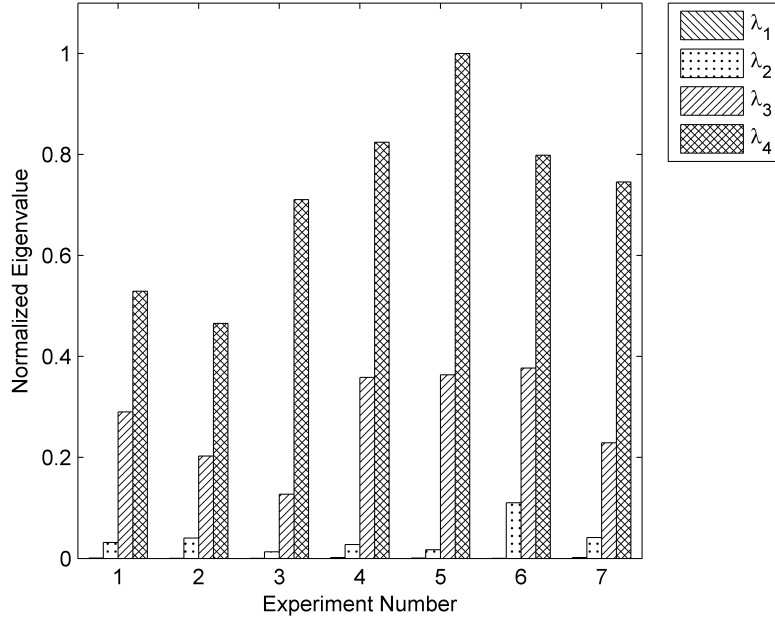


Figure 4.18: Eigenmode gains for $n=4$, OFDM Tone 1.

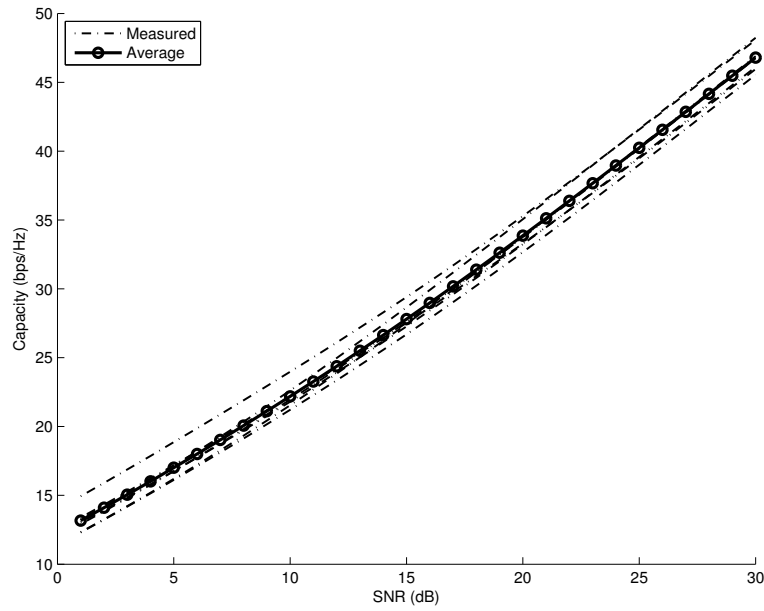


Figure 4.19: Capacity for several multipath experiments, OFDM Tone 1.

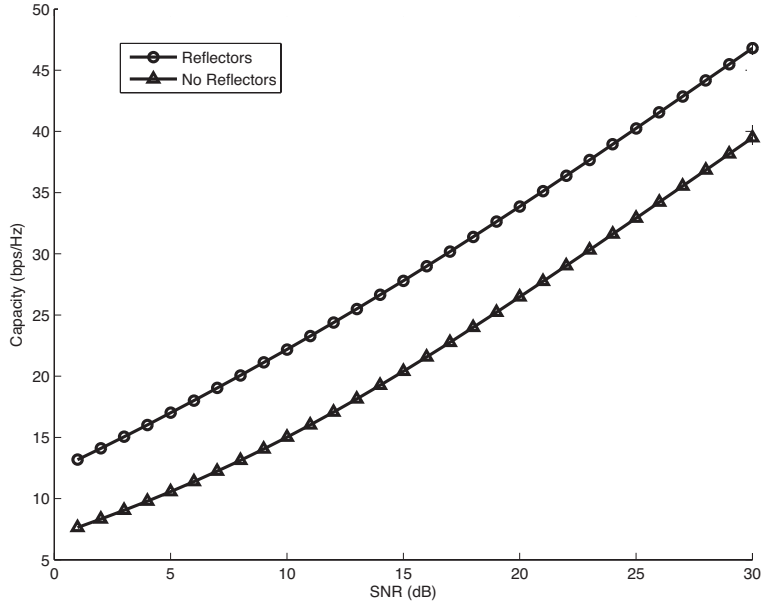


Figure 4.20: A comparison of average capacity with and without reflectors.

without test cases A and B respectively.

As expected, the measured capacity in Fig. 4.20 is lower without the use of reflectors thus justifying their use. The next section extends this study to compare the effect of MEA Element Spacing.

4.4.4 Varying MEA Element Spacing

A simple calculation finds the wavelength, λ , to be approximately 5 in. or 12 cm based on a 2.4 GHz carrier. The coherent distance is then approximately 2.5 in. The results thus far assume an element spacing of 5 in. with the broadside arrangement of antennas. As described in 4.3, this study is extended to analyze the effect on capacity when this distance is reduced closer to the coherent distance, namely test cases A, C and D.

Fig. 4.21 shows the average between several experiments for the 3 test cases (OFDM Tone 1), using a broadside antenna arrangement. To give an indication of the channel response, Fig. 4.22 illustrates the associated average eigenmode gains to this capacity. It is important to note that the transmitter signal power, and transmitter and receiver front-end gains remained constant as the MEA element distances were varied.

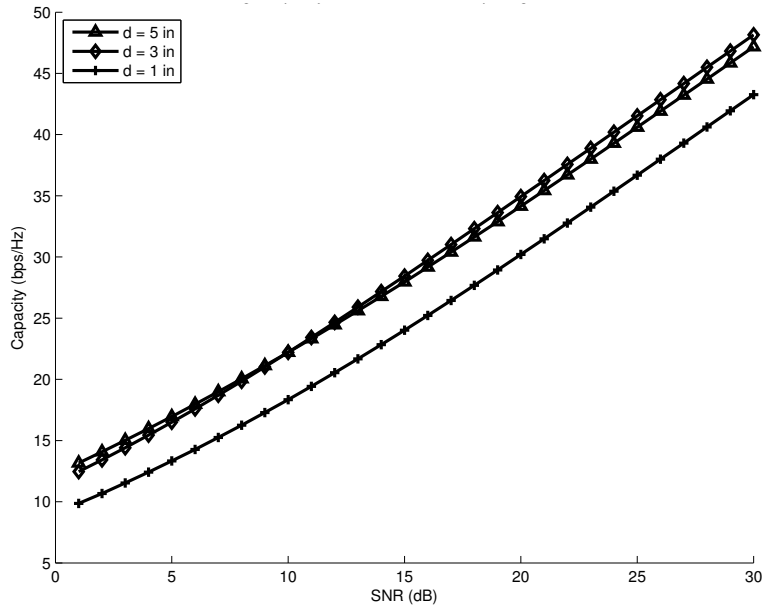


Figure 4.21: A comparison of average capacity for $d=1$ in, 3 in, and 5 in., OFDM Tone 1.

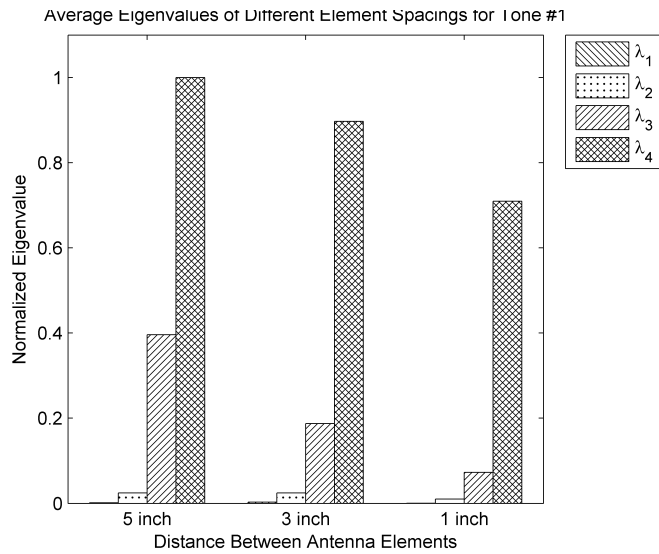


Figure 4.22: A comparison of average eigenmode gains for $d=1$ in, 3 in, and 5 in., OFDM Tone 1.

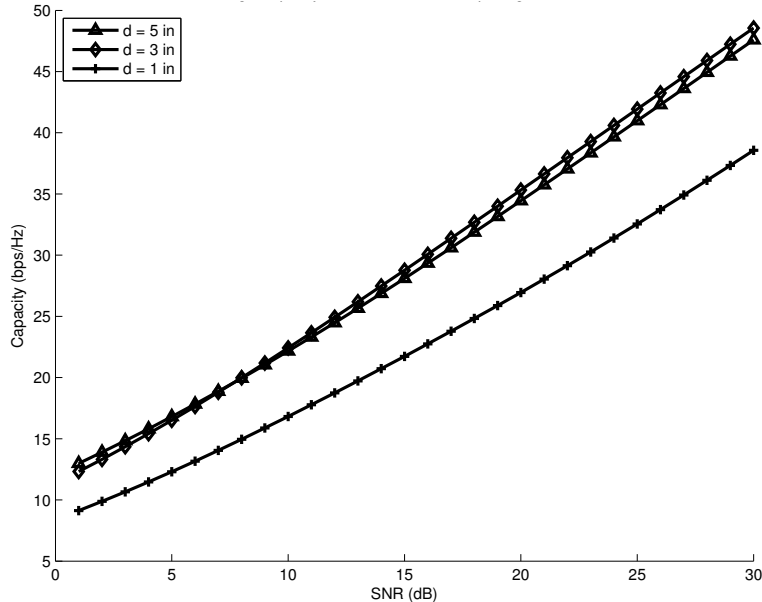


Figure 4.23: A comparison of average capacity for $d=1$ in, 3 in, and 5 in., OFDM Tone 52.

It can easily be seen in Fig. 4.22 that there is a significant reduction in eigenmode gains as the distance is reduced. It is also shown in 4.21 that the capacity drops considerably when the distance, d , drops to 1 in.—below the coherent distance

Fig. 4.23 illustrates a similar effect on the capacity. But, it can further be observed that on this tone the $d=1$ in. also leads to its capacity plot having a lower slope. This indicates not only a lower overall capacity, but a smaller capacity gain for improved SNR.

4.4.5 A Comparison to Previous Work

In related studies and literature, capacity is often benchmarked for the common case of 10 dB SNR in an indoor environment. For a separation of 3 in. and 5 in. between MEA elements, the spectral efficiency of our MIMO-OFDM implementation is on average between 20 bps/Hz to 25 bps/Hz. These results are in line with those presented in [3] and [13].

4.4.6 Design Challenges and Difficulties

In our study, two key difficulties prevent further characterizing the MIMO channel. After studying the effect of varied MEA element spacings at the receiver node, the logical next step would be to study the effect of varying the spacings at the transmitter. As mentioned

above, the testing procedure required the calibration of the receiver node for each experiment. It was found that varying the transmitter MEA spacings also varied the SNR a great deal so much so that the system would have to be re-calibrated. While recalibration of our receiver node was within the scope and ability of the design, the RFFE gains would not remain consistent. As a result, it would not be possible to maintain constant signal power levels to allow for a practical comparison between experiments. Consequently, the scope of our study was left to only study MEA spacings at the receiver.

Additionally, it was initially planned that the SNR be varied from the transmitter node and the overall capacity studied empirically in its entirety. This would also involve simultaneously measuring the SNR at the receiver. It was found that the hardware chosen as the RFFE added a parasitic noise making it difficult to measure the true noise power of the channel. Further research may be required into possible filtering techniques to allow for this study.

Chapter 5

Conclusions and Future Work

As current W-LAN and 3G cellular technologies reach their limits, engineers and manufacturers are looking for new ways of increasing QoS and spectral efficiencies to support services such high-definition videoconferencing and ubiquitous service coverage. MIMO technologies prove to be a promising step toward meeting tomorrow's demands by leveraging space diversity to increase throughput and reliability of a wireless link. Current technologies allow for up to 54 Mbps for W-LAN and between 8 Mbps to 11 Mbps for mobile cellular devices. MIMO technologies allow for spectral efficiencies 20 times that of today's infrastructure, thus potentially improving current data rates also by this factor. Conventional test methods, however, would have to be revised for newer cross-functional methodologies combining RF, antenna, and baseband hardware and software. Thus the adoption of MIMO brings with it new testing and implementation challenges.

In this dissertation, a novel design for the rapid implementation of a MIMO OFDM-based platform was presented. This platform allows for data to be transmitted in real-time from a source to a receiver node in a constructed multipath environment. It was first shown that the MIMO channel can be characterized in terms of its channel impulse response for various independent multipath arrangements. The channel was then analyzed and decomposed into parallel eigenmodes with associated gains. Finally, the capacity of the system was analyzed for various MEA separations.

In conclusion, the impact of the study is the following: There is an inherent need for the rapid development of devices to meet market demand; our implementation demonstrates this ability through the use of a FPGA/DSP-Hybrid platform. In addition, the

results from the presented study illustrate that while the channel impulse response varies significantly between experiments, the capacity, however, remains consistent. This implies that it is possible to achieve a reliable estimate of the capacity of the MIMO wireless link. Additionally, the significant reduction in capacity seen as the MEA spacing is reduced below the coherent distance demonstrates its impact on system performance. Spectral efficiencies of 20 bps/Hz to 25 bps/Hz were seen for MEA separations above the coherent distance, consistent with related studies. Results from separations below this distance were found to be 5 dB to 10 dB lower. Pushing separations further above the coherent distance was beyond the scope of this research, but motivates further study.

This study made the assumption of constant noise power across receiving antennas and across OFDM subcarriers, as also seen in other research. Further investigation is required as to the impact of varying noise levels. In addition, examining methods for leveraging CSI at the transmitter would also be of benefit to achieving even higher spectral efficiencies. Lastly, MIMO gains can further be explored through the use of beamforming, advanced antenna selection and space-time coding.

Bibliography

- [1] "Measuring the Information Society, *International Telecommunications Union, ITU-D*, 2010, Geneva, Switzerland.
- [2] William Webb, *The Future of Wireless Communications*. Norwood, MA: Artech House, Inc., 2001.
- [3] G.J. Foschini, "Layered Space-Time Architecture for Wireless Communication in a Fading Environment When Using Multi-Element Antennas, *Bell Labs Technical Journal*, October 1996.
- [4] F. Liang, "The Challenges of Testing MIMO", *Next-Generation Wireless*, November 2005, pp. 20-28.
- [5] S. M. Alamouti, "A Simple Transmit Diversity Scheme for Wireless Communications, *IEEE Journal on Selected Areas in Communications*, February 1998, pp.17-24.
- [6] S. Mangold et al., "IEEE 802.11e Wireless LAN for Quality of Service," *Proceedings of the European Wireless*, Vol. 1, pp. 32-39, Florence, Italy, February 2002.
- [7] *Supplement to IEEE standard for telecommunications and information exchange between systems LAN and MAN specific requirements Part 11: Wireless LAN MAC and PHY specifications: High-speed physical layer in the 5 GHz band*, IEEE Std 802.11a-1999.
- [8] G. Tsoulos, *MIMO System Technology for Wireless Communications*. Boca Raton, FL: Taylor & Francis Group, 2006.
- [9] M. Jankiraman, *Space-Time Codes and MIMO Systems*. Norwood, MA: Artech House, 2004.

- [10] G.J. Foschini, M.J. Gans, "On limits of wireless communications in a fading environment when using multiple antennas, *Wireless Personal Communications*, vol. 6, March 1998, pp. 311-335.
- [11] E. Telatar, "Capacity of Multi-Antenna Gaussian Channels, *European Transactions on Telecommunications*, Vol. 10, No. 6, November/December 1999, pp. 585-595.
- [12] V. Tarokh, "SpaceTime Block Codes from Orthogonal Designs, *IEEE Transactions on Information Theory*, Vol. 45, No. 5, July 1999, pp. 1456-1467.
- [13] D. Chizhik et al., "Effect of Antenna Separation on the Capacity of BLAST in Correlated Channels," *IEEE Communications Letters*, Vol. 4, No. 11, November 2000, pp. 337-339.
- [14] A. van Zelst et al., "Implementation of a MIMO OFDM-Based Wireless LAN System," *IEEE Transactions on Signal Processing*, Vol. 52, No. 2, February 2004, pp. 483-494.
- [15] G. Tsoulos, *MIMO System Technology for Wireless Communications*. Boca Raton, FL: Taylor & Francis Group, 2006.
- [16] T. M. Cover and J. A. Thomas, *Elements of Information Theory*. Chichester, U.K.: Wiley, 1991.
- [17] T. Choi and S. M. Alamouti, "Comments on Ergodic and Outage Capacity," *IEEE Presentation on 802.11*, January 2004.
- [18] M. Chiani et al., "On the Capacity of Spatially Correlated MIMO Rayleigh-Fading Channels," *IEEE Transactions on Information Theory*, Vol. 49, No. 10, October 2003, pp. 2363-2371.
- [19] *Quad Dual Band RF Transceiver Technical Reference Guide*, ComLab, October 2007.
- [20] *HyperLink Wireless brand HyperGain Range Extender 7 dBi Mobile or Desktop Omni Antenna with Magnetic Base Specification*, L-com, 2009.
- [21] J. Heiskala and J. Terry, *OFDM Wireless LANs: A Theoretical and Practical Guide*. Indianapolis, IN: Sams, 2002.
- [22] R. Wilson, *Propagation Losses Through Common Building Materials 2.4 GHz vs 5 GHz*. Magis Networks, Inc., August 2002.

Appendix A: System Architecture

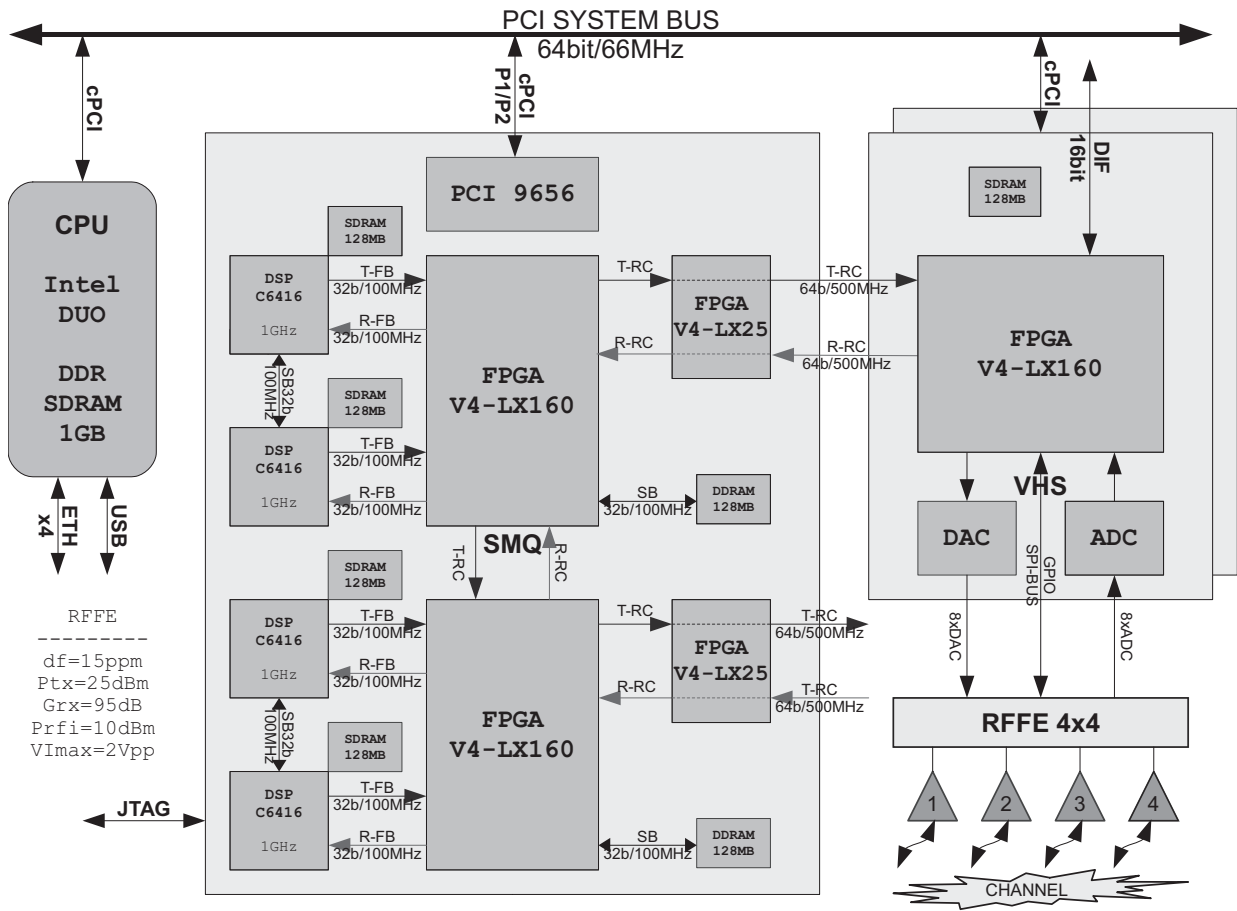


Figure 5.1: A schematic of a node's internal components and buses.

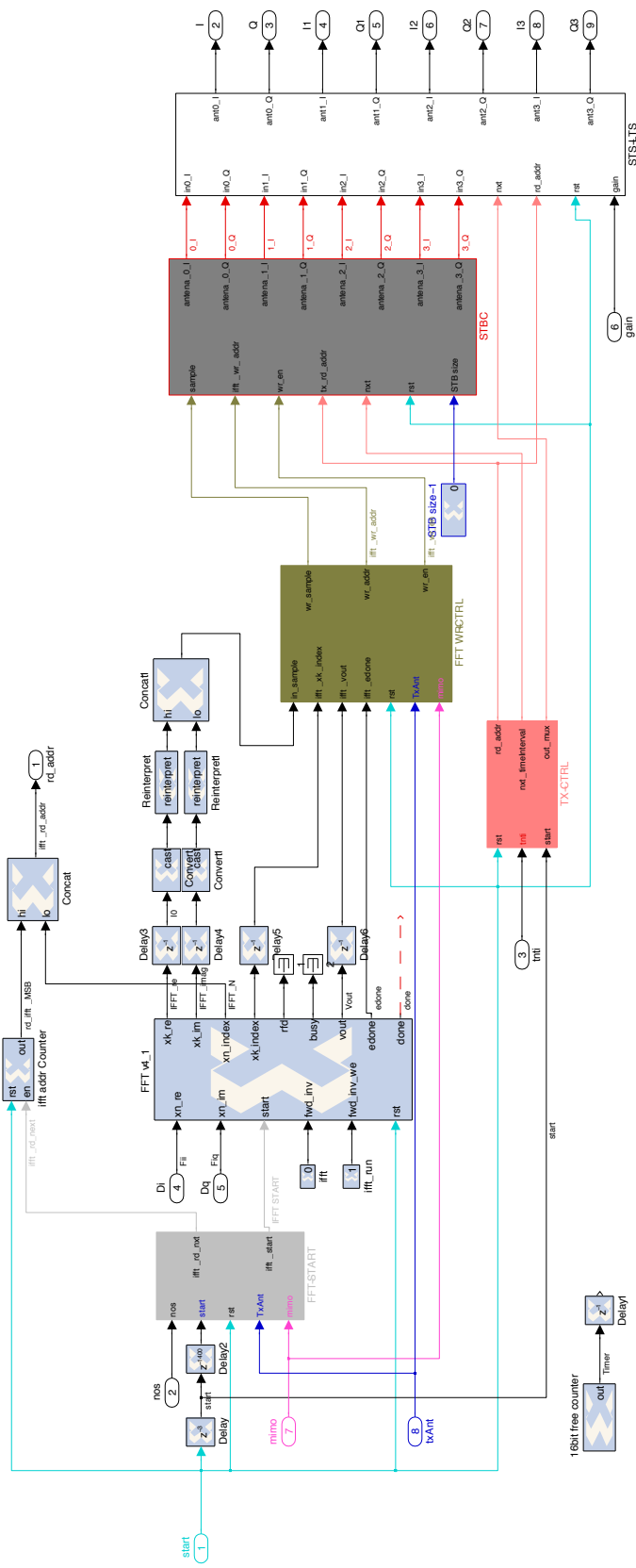


Figure 5.2: The Xilinx block-based TX design.

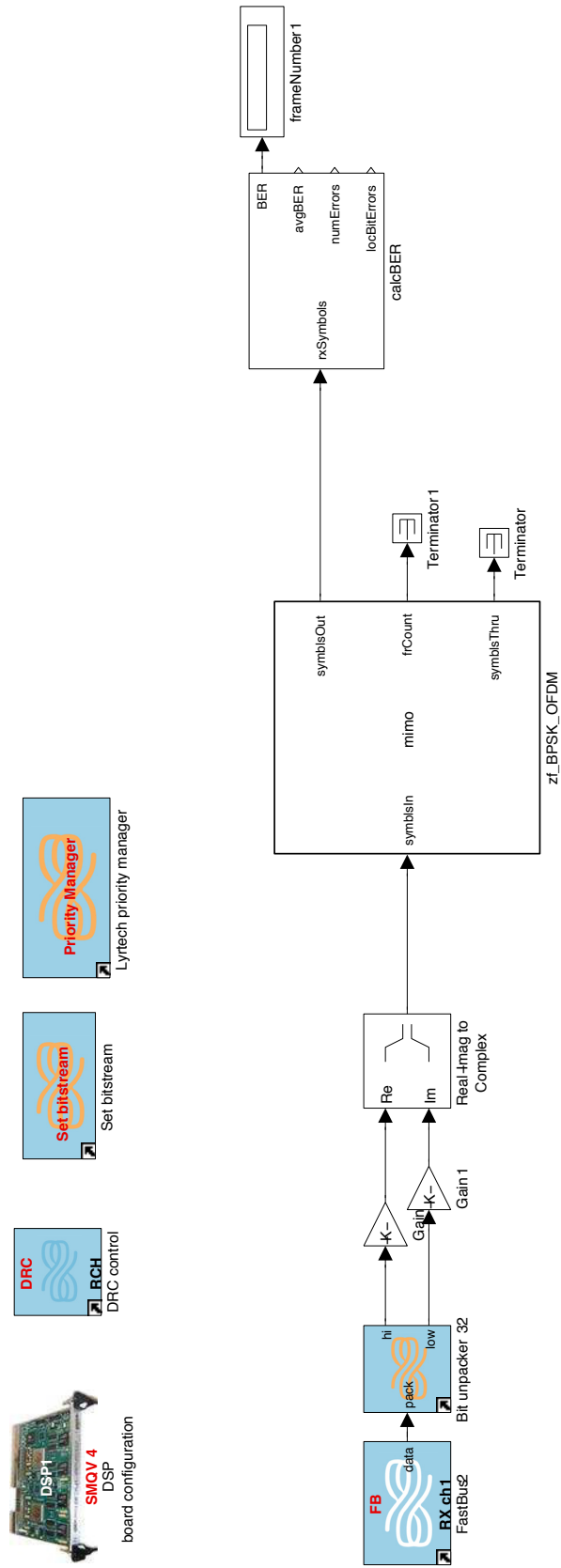


Figure 5.4: The Simulink block-based DSP design at the RX.

Appendix B: Testing Procedure

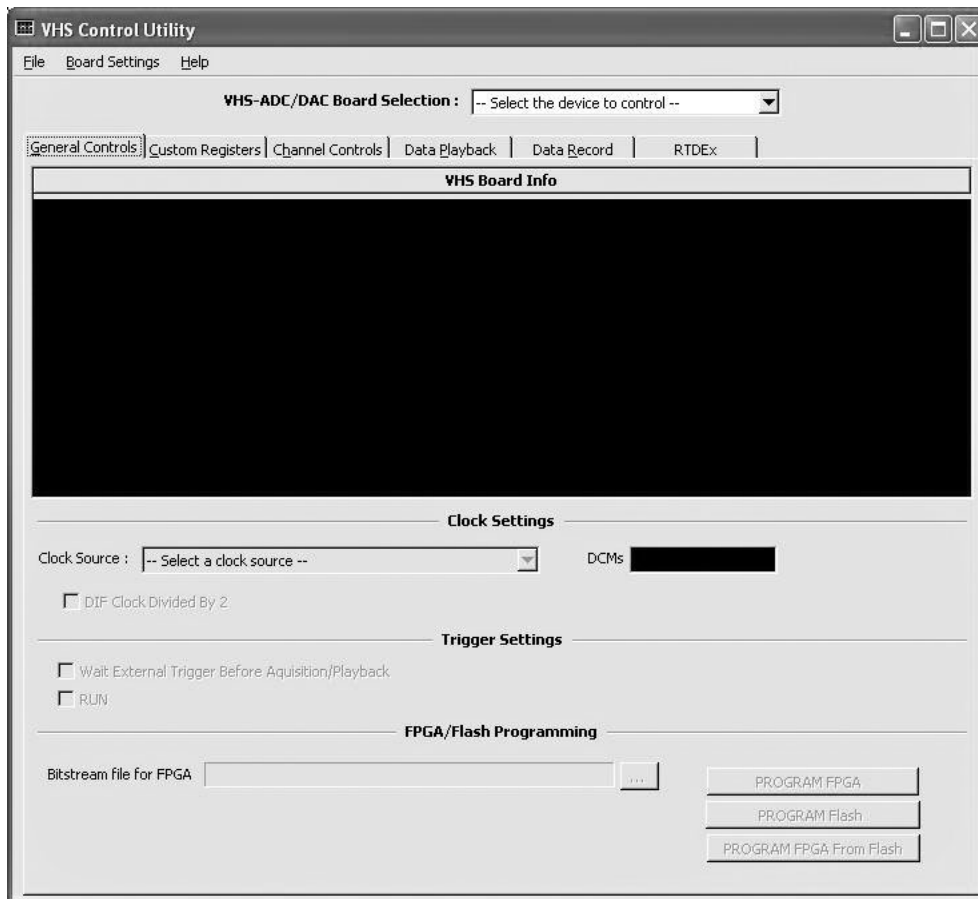


Figure 5.5: VHS Control Utility screenshot, programming the FPGA.

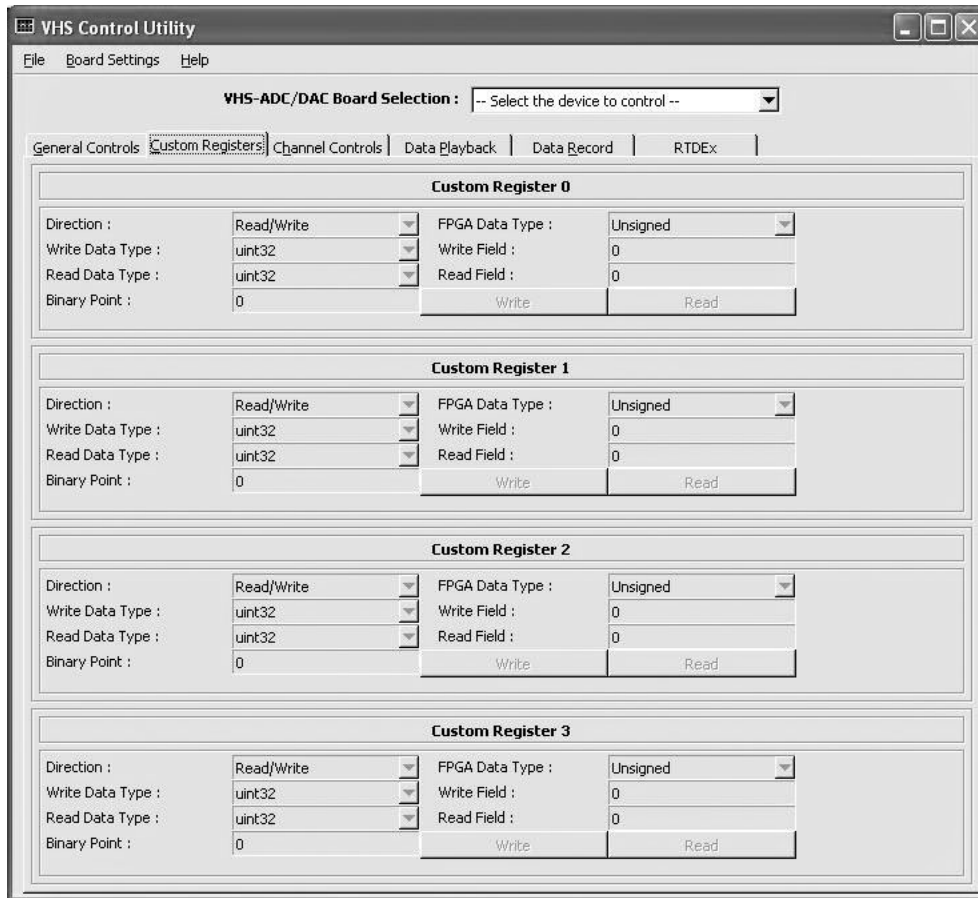


Figure 5.6: VHS Control Utility screenshot, setting control registers.

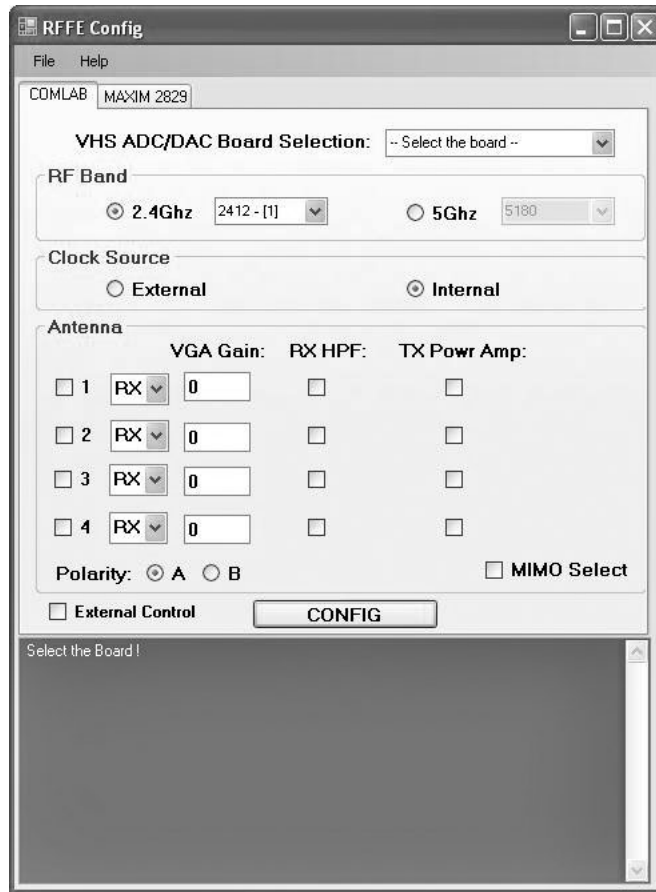


Figure 5.7: RFFE Utility screenshot.

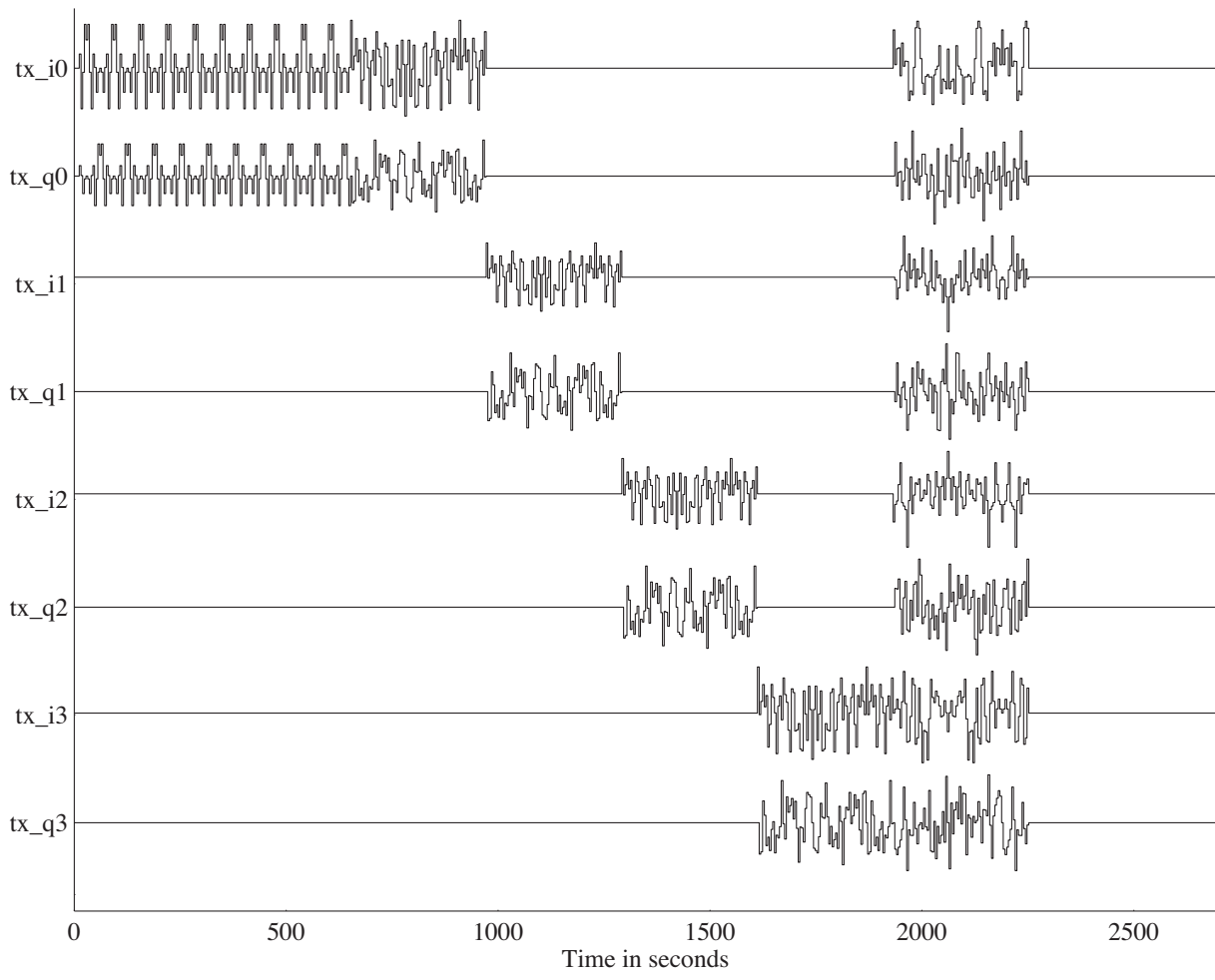


Figure 5.8: Typical off-air received signals.

Appendix C: Additional Test Results

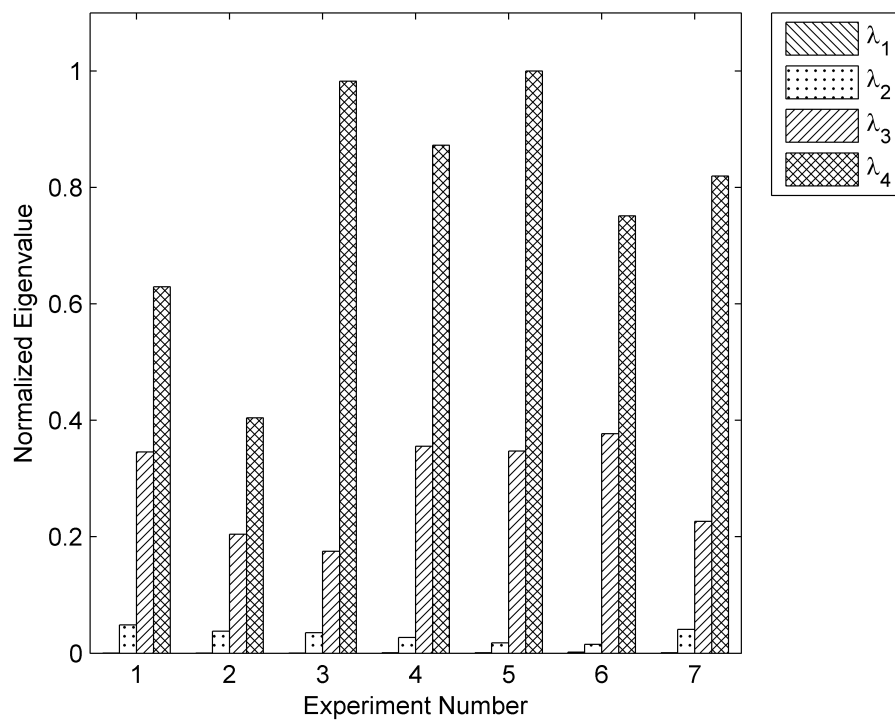


Figure 5.9: Eigenmode gains for $n=4$, OFDM Tone 26.

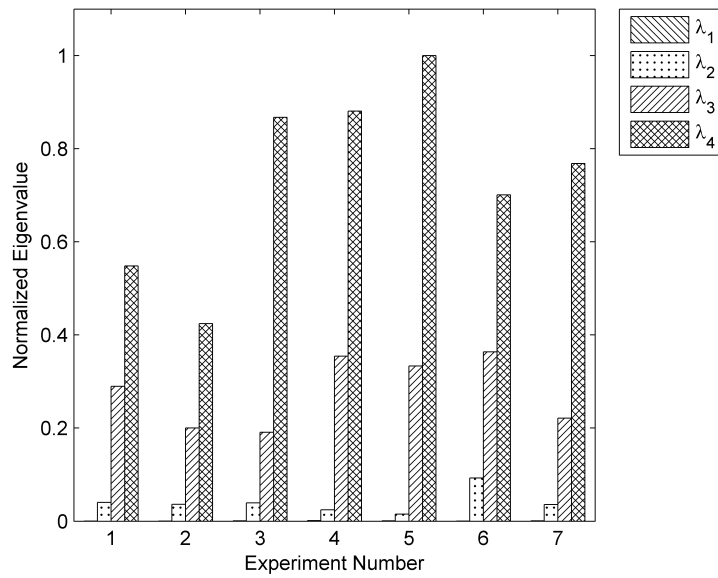


Figure 5.10: Eigenmode gains for $n=4$, OFDM Tone 52.

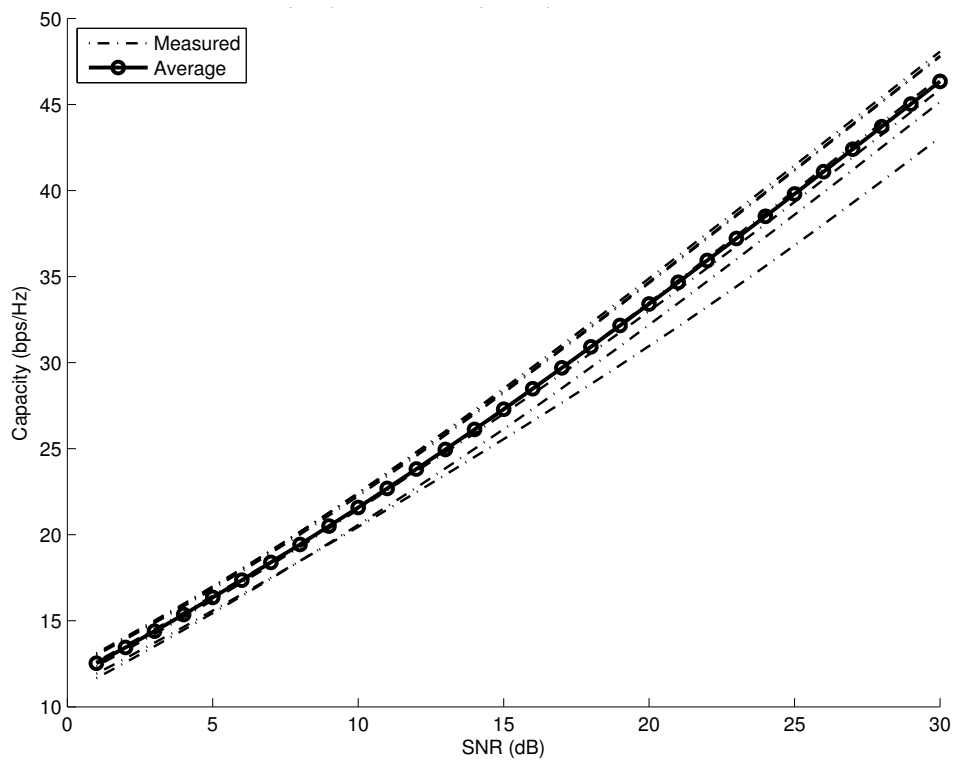


Figure 5.11: Capacity for several multipath experiments, OFDM Tone 26.

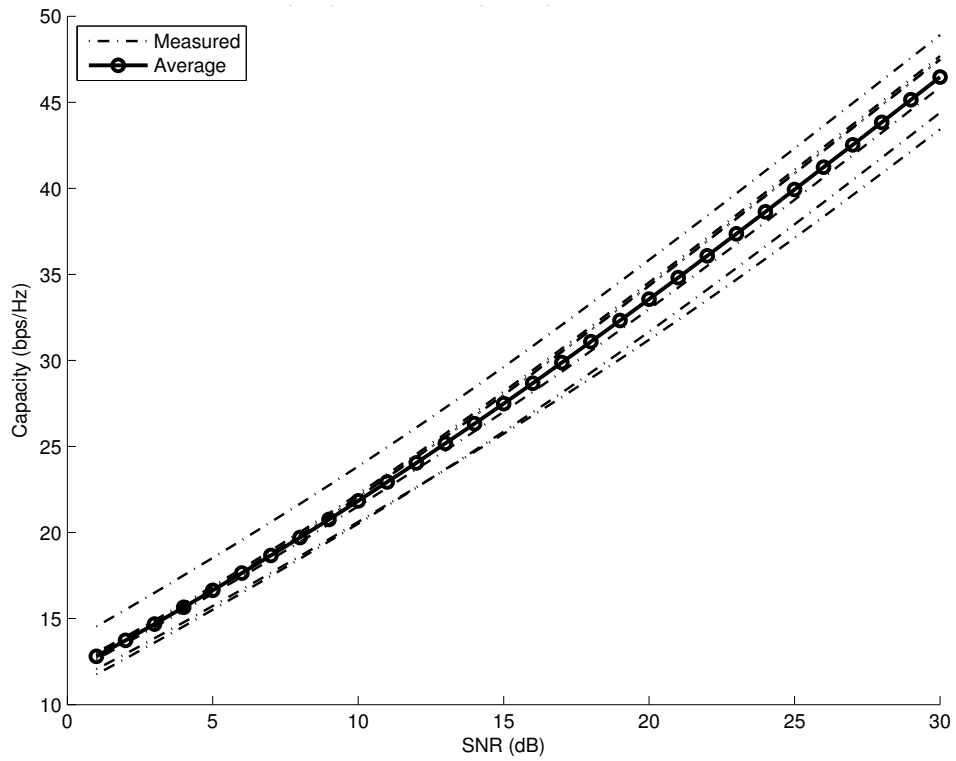


Figure 5.12: Capacity for several multipath experiments, OFDM Tone 52.